ADAPTIVE CONTROL FOR SOLAR ENERGY BASED DC MICROGRID SYSTEM DEVELOPMENT

by

Qinhao Zhang

B.S. Shanghai Jiao Tong University, 2011

M.S. University of Pittsburgh, 2012

Submitted to the Graduate Faculty of

Swanson School of Engineering in partial fulfillment

of the requirements for the degree of

Doctor of Philosophy

University of Pittsburgh

2016

UNIVERSITY OF PITTSBURGH

SWANSON SCHOOL OF ENGINEERING

This dissertation was presented

by

Qinhao Zhang

It was defended on

December 3, 2015

and approved by

Zhi-Hong Mao, Ph.D., Associate Professor

Gregory Reed, Ph.D., Professor

Yiran Chen, Ph.D., Associate Professor

Thomas McDermott, Ph.D., Assistant Professor

William Stanchina, Ph.D., Professor

Mingui Sun, Ph.D., Professor

Dissertation Advisor: Zhi-Hong Mao, Ph.D., Associate Professor,

Gregory Reed, Ph.D., Professor

ADAPTIVE CONTROL FOR SOLAR ENERGY BASED MICROGRID SYSTEM DEVELOPMENT

Qinhao Zhang, PhD

University of Pittsburgh, 2016

During the upgrading of current electric power grid, it is expected to develop smarter, more robust and more reliable power systems integrated with distributed generations. To realize these objectives, traditional control techniques are no longer effective in either stabilizing systems or delivering optimal and robust performances. Therefore, development of advanced control methods has received increasing attention in power engineering. This work addresses two specific problems in the control of solar panel based microgrid systems. First, a new control scheme is proposed for the microgrid systems to achieve optimal energy conversion ratio in the solar panels. The control system can optimize the efficiency of the maximum power point tracking (MPPT) algorithm by implementing two layers of adaptive control. Such a hierarchical control architecture has greatly improved the system performance, which is validated through both mathematical analysis and computer simulation. Second, in the development of the microgrid transmission system, the issues related to the tele-communication delay and constant power load (CPL)'s negative incremental impedance are investigated. A reference model based method is proposed for pole and zero placements that address the challenges of the time delay and CPL in closed-loop control. The effectiveness of the proposed modeling and control design methods are demonstrated in a simulation testbed. Practical aspects of the proposed methods for general microgrid systems are also discussed.

TABLE OF CONTENTS

LIST OF TABLES

LIST OF FIGURES

PREFACE

I would like to thank my advisors, Dr. Zhi-hong Mao and Dr. Gregory Reed, for their sincere effort and guidance in every aspect of my training. They showed me how to become a professional, insistent and hardworking scholar. Your experience and knowledge have inspired me to choose electrical power engineering as my career.

I would like to thank all of my friends in the research lab and outside as well. You constantly help me in different aspects whenever I experience challenges. Especially, my sincere thanks to Brandon, Raghav, Shimeng, Joey, Alvaro, Pat, Ansel, Matt and Hashim. Meanwhile I would also like to thank Xiao Li and Bojian Cao for your kind and generous help, which has greatly touched me.

I would like to thank all my dissertation committee members, Profs. Yiran Chen, Thomas McDermott, William Stanchina, and Mingui Sun, for your valuable guidance and strong support. I am so glad and honored that I have chance to know each of you.

Last but not least, I would like to thank my family for always being supportive to my choices and believing in me.

1.0 INTRODUCTION

With the reduction in supply of conventional energy resources on this planet, it is critical and necessary to launch an investigation into renewable energy for a sustainable future. The United States Department of Energy (DoE) projects that the U.S. will receive 20 percent of the its energy supply from renewable energy by 2030 [1]. This is equivalently to around a 300 GW capacity. Recently in Europe, wind generators have been constructed offshore of Denmark. With the rise of renewable energy, the configuration of power systems will have to change accordingly. Therefore, more advanced control techniques are needed for addressing the issues occurred in a renewable or hybrid power system. There may also need to improvements to energy conversion efficiency so that more energy can be extracted from the renewable energy resources. This dissertation is going to present the power module of MPPT and also examine the time delay issue that occurs in the microgrid or medium voltage DC system.

Currently, the grid is in the process of upgrading. The goal of such upgrade is to ensure that the next generation grid is more resilient and smarter in dealing with voltage and power fluctuations. With such high performance required in power regulation, it is critical to eliminate any stability issues caused by a constant power load. This work is going to present a comprehensive method of addressing the constant power load in the system.

1.1 TOPIC OF THE DISSERTATION

MPPT improvement and realization:

Solar and wind energy are promising energy resources especially considering the amount of the resource, the cost, and other environmentally friendly considerations. Many signs such as government incentive policies, the increasing construction of large solar power plants in the Middle East and the large manufacture amount of solar panels point to the conclusion that renewable energy is going to be the dominant source of future energy. Currently, the efficiency of converting solar energy to electrical energy is around 12-22%. The energy conversion ratio range is from residential solar panel, which is around 14% to spacecraft's solar panel's application which is around 22% [2]. To improve the conversion ratio significantly, it requires the development of a new photon material in order to convert solar to electrical energy more efficiently. It would be highly beneficial to develop a maximum power point tracking algorithm which will facilitate energy extraction as we noticing that the solar irradiance is randomly changed. Basically, these are the two dominant reasons are contributing the low energy conversion ratio. The former is the more important factor though the latter can also contribute to higher energy production.

MPPT is an optimization-based algorithm designed to find the maximum power point operating point on the load side. This algorithm is primarily applied to unimodal systems and its goal is finding the extreme point within a system. Unimodel system means that there has only one extreme points, either maximum or minimal point within the system. And therefore we can guarantee by using the MPPT, we are able to track the extreme points in the system. Solar panel possess many unimodal characteristics but bring other potential challenges, for example, when there are multiple extreme points such as when a shadow is cast over the panel. In this work, the

shadow problem will not be discussed. The less time it takes to find the extreme/optimal point, the better the efficiency of the solar panel it will have. Since the overall amount of solar energy that can be exploited will be huge, even a 1 percent improvement of energy conversion would bring considerable profit and energy savings.

One of the major applications of MPPT is solar and wind where there is only one extreme point in the system. Despite decades of research and analysis, there is still no ideal algorithm for tracking the maximum power point due to two factors: cost and efficiency. This dissertation will propose using the ripple correlation control MPPT algorithm for locating the maximum power point and the use of another control algorithm to better improve the transient dynamics of the solar panel once a new duty cycle is found.

Adaptive Control Theory

Most application of control algorithms is for the system with small time constant and provide accurate and fast control effort. On the contrast, control techniques in the power electrical systems are not as critical as many other applications and the reason is because time constant of power system is large, namely, the system is slow to control and therefore it doesn't require fancy control algorithm for high performance of control object. However, with the integration of power conversion system based on power electronics device, the time constant and system time constant become much faster. And therefore it requires certain type of control technique to satisfy this application, such as the adaptive control or optimal control techniques [3-6]. The basic infrastructure of current AC power grid is under development and, as a result, it has lots of issues need to be regulated with better solution and stability. One current prevalent control algorithm is PID control. PID control represents three control actions: proportion,

integration and derivation control. Proportion control has advantages of fast system response; integration control eliminates steady state error and achieves better control objectives. Derivation control tunes the oscillations and overshoot performance during the transient dynamics. It should be noted that derivation control is always designed with the low pass filter as the derivation term is going to cause instability by high frequency noise.

In summary, it is prevalent and useful to implement the PI control in the power system application[7, 8]. Power systematic level of control involves of automatic generation control (AGC) or many other slow control scheme[9]. While as the penetration of renewable energy, there are power electronic based modules are integrated to the power grid. The typical control strategy for control these modules as the output is sinusoidal waveform, it uses Park transformation (dq transformation) to switch the control objects into two constant values. The internal dynamics and also potential problems caused by IGBT and MOSFETs are more difficult to deal with compared to some other device/switches. The reason is because these high performance semiconductors have lots of nonlinear characteristics and the conventional PI controller's design will not fit these situation as we assumed that the analyzed system is given and static. And to address this problem, lots of modern control technologies/algorithms will be developed.

Adaptive control theory is one branch in the modern control domain. It was firstly introduced in 1950's. In the territory of adaptive control, model reference adaptive control is one important method to effectively solve complex nonlinear system. Literally, controller's parameters are adaptively changed according to the operating points in the system. In the adaptive control regime, it uses Lyapunov function to design the controller such that the systematic error follows the stability in term of Lyapunov stability and the error will

asymptotically approaches to zero[10, 11]. The beauty of using model reference adaptive control in many engineering applications lies in adaptive control doesn't necessary require complete information of the system for developing controller algorithm. And such advantage is very critical in the power electronic device based module development because the system's characteristic is various or unobtainable due to the nonlinearity characteristic of the system. By integrating this algorithm into the MPPT development, the performance improvement has been realized. As shown in the following chapters, adaptive control law is decoupled to the MPPT algorithm in the solar panel and the more satisfactory transient performance in the solar conversion system achieved.

Stability issue in the medium voltage DC microgrid transmission system

The rise of the renewable variable generator is also accompanying the rising development of DC microgrid construction. The development of the hybrid power grid has many renewable generators entering the AC system. When many power electronic inverters and motor drives are tightly regulated they act much like constant power loads. Constant Power Load (CPL) has a negative impedance increase while the relationship between the changes of voltage versus the change of current is negative, namely negative incremental impedance instability.

And lots of power electronic inverters and motor drives, when they are tightly regulated, then they act like constant power loads. Constant Power Load (CPL) acts as a negative incremental impedance in the system dynamics. It provides instability to the overall electric power system and due to the more usage of constant power load applications in the field, it is urgent and important to come up solution for stabilizing such phenomena. Meanwhile, centralized control is utilized for power transmission system deployment by mean of automatic

meter instrument (AMI). AMI collects the power system data, such as voltage and current measurements, and then sends the collected data back to the DMS for deployment plan computation. We are able to control the power flow demand by mean of control the energy resource, such as the pitch of the blade in wind generators or through the duty cycle which is fed to the converters/inverters. In this work, the focus is merely on the duty cycle which is more versatile in application. And in a nutshell, such control topology forms one close feedback loop for the system's configuration. In practice, we found that there has time delays within the system and as a result, the voltage output of the converter becomes instable. And thus it is also critical to find a solution to get rid of the potential influence or instability caused by the time delay. And by mean of adaptive control and modern control, it is able to eliminate the instability.

This dissertation is to explore the potential solution for improving power grid configuration with more reliable and efficient controller development by using modern control techniques. Such development is aligned with the expectation from people who wants our power grid to become more powerful, smarter and more robust. And in the following Chapters, the details will be discussed. In the Chapter 2, it will show the state of arts for the given technologies and explanation of why we need more advanced solution to address these situation better; in Chapter 3, it is going to present the method which solve the problem and its related mathematical development and derivations. In Chapter 4, it is going to show the results of the system by using and without using our proposed methods. Several comparison in quantity and quality are going to be discussed. In Chapter 5, it is going to discuss the overall work and some future potential improvement on how to design the system even better.

2.0 LITERATURE REVIEW

The upgraded Power grid is upgrading to be smarter, more robust, and more resilient. The reason is because there will be more dynamics within the power system due the increasing number of variable generators entering the grid. Meanwhile there is the rising practice of installing power electronic devices with different rating settings into the system for different applications. Dynamics from different elements are going to destabilize the power system and also create more potential problems. Although these topics are not going to be covered in this dissertation work, several obvious changes are going to take place: harmonics, voltage regulation, variable distributed generator's impact on the system.

One of the appealing features of the next generation of the grid is that it will be designed to be much more resilient and smarter in order to handle the issues when there are fluctuations in the power system. As a result, more power with a decent power factor or power quality will be delivered with a steady voltage profile. Another feature of the grid is that it will consist of a much higher percentage of renewable power resources supplied locally. Since the availability of power sources can be localized, according to the geographic resources distribution, a local power supply can be provided without remotely connecting to the main power grid. Such a method of planning will benefit many regions which are either lacking a convenient supply of sustainable energy or are cut off from the main grid as the result of a nature disaster. There are two major components of the renewable power supply so far: solar energy, which can be extracted and

converted to electricity by using solar panel; and wind, which can be extracted by wind power generators. Wind power generators use wind blades to extract energy through wind and produce the AC energy.

There are opportunities and challenges from these energy sources: 1). These energy resources are free and unlimited; 2). The involve power electronic devices and the come with harmonic components within the system; 3). They require many regulators to control the voltage output and therefore typically can be treated as a constant power load; 4). Since wind and solar is randomly distributed it therefore requires forecasting to avoid voltage spikes in the system. For example, the weather often changes significantly during one day alone. The solar energy source profile is very likely to align to the load consumption profile whenever there is a sunny day, it is also less likely to have lots of wind. Somehow the wind resource profile is aligned opposite of the energy consumption profile in the system. One of the significant advantages to using renewable energy is that the energy source is plentiful and great enough to extract. Therefore in order to most efficiently extract and convert solar energy into electrical energy the conversion ratio needs to be high. By using of different control and regulation methods, these energy generators act like constant power load. As mentioned earlier, the negative incremental impedance leads to the stability of the system. Therefore we need a solution to address this issue.

2.1 MPPT ALGORITHM

Solar panel's voltage/current versus power output characteristic is a unimodal without considering the shadow situation. With changing parameters, such as the working temperature and solar irradiance level, there is always one unique extreme point in the P-V curve. The maximum power point tracking algorithm (MPPT) is supposed to enable the solar panel to always operate at the nominal voltage magnitude. And therefore the power output will be at its maximum. The Maximum Power Point Tracking algorithm is pretty well-known algorithm in the industry for at least two decades [3]. Its major contribution to the power system, specifically, is that it finds the maximum power point when the system carrying the nonlinearity characteristic. For example, solar panels are distributed variable generators because they are more sparsely installed in the field and also because the output of the solar panels is directly related to solar radiation. in Figure 1, it shows the characteristic of the I-V curve of solar panel, which the maximum power point lies at the "knee" point of the curve. The contribution of MPPT is that the controller always tracks the maximum power point under the different scenarios. As shown in Figure 1, the external environment has two settings: different solar irradiance and different working temperatures. Red curve represents the solar irradiance being $750\ {}^{W}/_{m^2}$ and the blue curves represents the solar irradiance being $1000\ {}^{W}/_{m^2}$. The solid line represents the temperatures of the solar panel being 25 Celsius degree and the dashed line represents the temperature of the solar panel being 40 Celsius degree. It is not quite obvious to observe the maximum power point is corresponding to different voltage value barely based on the upper sub-figure, however, it is quite straightforward to notice that the maximum power point locates at

different voltage value if observing the P-V curve carefully. Solar panels are distributed variable generator as they are they are more sparsely installed in the field and also the output of the solar panels are directly related to the solar irradiance.

In practice, there are two topologies of the solar panel configurations: one is a stand-alone PV plant while the other one is grid tied PV plant. The difference between these two types of configurations lies in whether or not it is necessary for the PV generator to send and receive energy to and from the power grid. In the stand alone PV panel, it usually goes through the MPPT algorithm first. This algorithm is used to calculate the duty cycle when there is a change in the external environment. Then, there is a power converter which is going to elevate or decrease the voltage output and make the voltage magnitude match the load requirement.

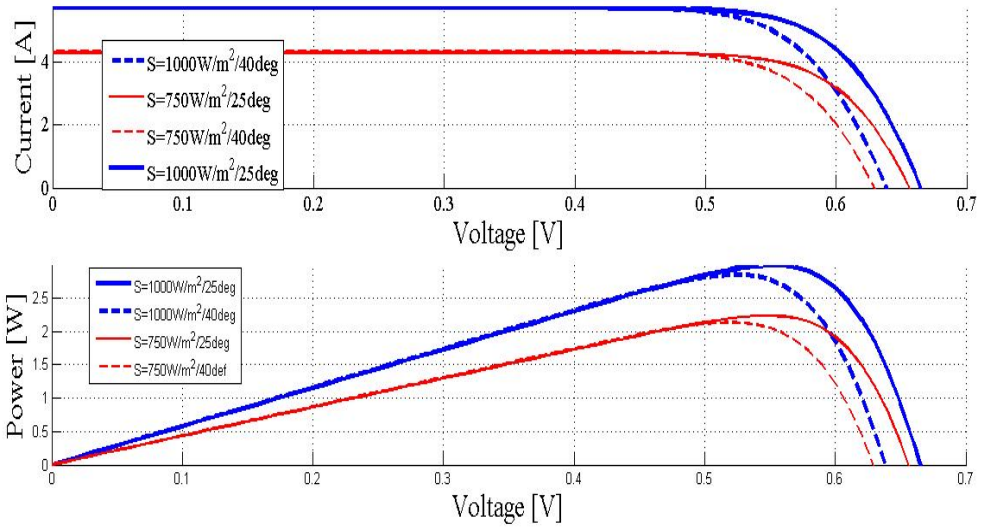

Figure 1: I-V curve and P-V curve of the solar panel.

The efficiency improvement of the power conversion system can significantly increase the power energy converting ratio by only one percentage point. The usage of solar energy will be unlimited.

Several MPPT algorithms have been reported in the literature. The most common algorithm is perturb and observe method [12, 13]. This control strategy requires external circuitry to repeatedly perturb the voltage array and subsequently measure the resulting change in the output power. P&O is a proven technology and has been intensively used in an industry application. The advantage of P&O is that it is cost effective and relatively easy to implement. However, the algorithm is inefficient in the steady state because it needs a ripple component of the current and voltage. This in turn, requires extra energy for the purpose of searching for the optimal operating point. This method is also very inefficient as searching requires large consumption of energy. The P&O algorithm also fails under rapidly changing environmental conditions. This is because it cannot discern the difference between changes in power due to environmental effects versus changes in power due to the inherent perturbation of the algorithm.

The Incremental Conductance Method [14, 15] uses the fact that the derivative of the array power with respect to the array voltage is ideally zero at the MPP. Specifically, when the sign is positive, it means that the current operating point lies to the left of the MPP. On the other hand when the sign is negative, it means that the current operating point lies to the right of the MPP. This method has been shown to perform well under rapidly changing environmental conditions, such as in the shade of solar radiation, nevertheless it comes at the expense of increased response time due to complex hardware and software requirements. These then become the major drawback of this algorithm.

In [16, 17], the author mentioned an important issue concerning the existing PV panels in the field. The major concern is that the partial shading due to clouds, trees, buildings or overheads, such that the bypassed diodes across modules may make the system difficult to track the solar curve using the MPPT scheme. Therefore the curve of P-V or I-V in the solar panel exhibits a twisted curve when the external environment behaves as such. Since the characteristics of the solar panel's operating point varies, the global extreme point in the solar panel is going to be hard to find because there are numerous local maximum and minimum power points appearing. The author presents a critical concern about the partial shading as a common cause of reduction in the power yield of a PV source. The author then presents the algorithm to solve the partial shading issue in the solar panel. This issue is very critical and has been ignored by many researchers because the solar panel is often assumed to be well exposed to the sunshine during it is working.

In [18, 19], a T-S Fuzzy Logic Controller is proposed to solve the MPPT algorithm for stand-alone solar power generator systems. The advantage of using the Fuzzy Logic Control algorithm is that such method provides robustness to the dynamics of the system. The underlying principle of fuzzy logic is that the nonlinear system can be represented as a series of IF-THEN fuzzy rules. These rules have local linearity characteristics to equivalently represent the nonlinearity characteristic of the solar panel as an entire system. Then the variation of the current and the voltage values will be sent to the table of fuzzy rules to determine the controlling signal. The control signal will modify the magnitude of the voltage or current in the panel such that the panel is functioning at the maximum power level. The advantage of this fuzzy logic control is that this algorithm facilitates the solar panel to have high conversion. However, the drawback of this algorithm is that those IF-THEN fuzzy rules are predefined, in other words, the characteristic

performance of the solar panel should be studied in detail so that the internal knowledge of the solar panel can be acquired. The information of the solar panel will be used afterwards to define these control rules. The characteristic of the solar panel may be quite numerous according to the manufacturer and it is very complicated to generalize the MPPT algorithm based on various solar panel brands and models. However, if it is assumed that all the PV panels are equivalently and follow the same principles, then the result of this algorithm is satisfied.

Here I listed one table to show the comparison of different given MPPT algorithms' pros and cons in Table 1. And it will give a clearer view of these algorithms. In general, there are many new algorithms proposed in the literature [13, 15, 17-28] and the goal is to improve the efficiency of the power conversion from the solar panel to the load side or, in some other cases, when the PV panel is connected to the grid. The golden rule in the engineering research follows the philosophy simplicity. Being smart and being good is always key in designing an electronic device. All of these algorithms, either has become the proven technology in the solar panel or are still under the research and development and they all have some flaws to some extent. Therefore it is very important to use different algorithms and methodologies to cope with these drawbacks.

Table 1: Comparison of MPPT Algorithms Characters.

MPPT Technique	Array Dependent	True MPPT	Analog/Digital	Convergence Speed	Implementation Complexity
Perturb&Observe Algorithm	*No*	*Yes*	*Both*	*Various*	*Low*
Incremental Conductance	*No*	*Yes*	*Digital*	*Various*	*Medium*
Fractional Voc	*Yes*	*No*	*Both*	*Medium*	*Low*
Fuzzy Logic Control	*Yes*	*Yes*	*Digital*	*Fast*	*High*
Rripple Correlation Control	*No*	*Yes*	*Analog*	*Fast*	*Low*
Current Sweep	*Yes*	*Yes*	*Digital*	*Low*	*High*
Slide Control	*No*	*Yes*	*Digital*	*Fast*	*Medium*

2.2 DEVELOPMENT OF MICROGRID INFRASTRUCTURE

As mentioned earlier, the development of the microgrid originates from each solar panel module. With sufficient renewable energy resource such as wind or solar, in future, it is going to have more and more distributed variable energy generators within the system. They are called a

microgrid and it can either provide energy as an independent system or it also can be connected to the AC system. Since the microgrid is much closer to the load site, whenever there is energy short from the microgrid, the AC system can also direct the flow the energy to the load side. This is similar to the grid-tied PV system which is able to receive and send energy to the grid. The microgrid shares the similar functionality.

The figure below shows the basic configuration of the hybrid power grid system in future. Within this system, when studying one section it can be simplified down to the system in Figure 10. In this figure, the left hand side represents the DC energy sources. The DC energy source is tightly regulated to produce constant power and there are constant power loads within the system. The plot of the constant power load V-I curve shows that there is a negative incremental impedance in the load and therefore it is going to produce within the system. There are two solutions to solve such an issue: one is to use the global control technique. For example this can be a slide mode control, a neural network etc. The other method is using much more conventional control technique and is called the linearization solution.

We linearize the nonlinear system at certain operating point and study the dynamic characteristic at that point.[29] The controller is designed and implemented for that certain operating point as well. In global sense of the system [30-32], the first method must be more versatile as it actually can address the problem with more freedom. However, in the real implementation of the control loop for the system, it encounters the time delay issue as in the control configuration of the power system. Within the physical construction of the power grid, there is a control configuration which is used to control the power grid's energy deployment plan. The control grid uses the data extracted and measured in the power grid nodes, such as the

automatic meter instrument or phase measurement unit (PMU), to develop the control plan by using the duty cycle in the converter connected to the DC energy generators.

In real time experiments, there is going to be a time delay within the control closed loop. The central server must calculate the duty cycle according to the measured data and send them back to the local SCADA communication tower. These towers will then send the duty cycle to the local converters. Within such a loop, the time delay is going to ruin the control effect as within the closed-loop. The feedback causes instability within the system and the results can be shown in a simulation. Therefore it is critical to point out that the time delay is a local situation and therefore it would be much more useful to use the linearization method rather than the global control technique to address the problem. It is suggested that users utilize the advanced control algorithm to change the poles and zeros of the system in order achieve a better system response overall. This dissertation is going to introduce several methods for addressing this problem in the following chapters. In each method, there are some advantages and disadvantages for the user. There is always a certain trade-off between the cost of the controller and the performance of the control effectiveness.

2.3 APPLICATION OF ADAPTIVE CONTROL IN POWER SYSTEM

Our goal for next generation power grid is to make the grid more reliable, more robust and smarter. These needs are correlated to the development of new features of power grid in future. There is going to have many more distributed small generators among the users and people are

going to interconnect the power grid with different types of renewable power generators to supply power energy to the users. In the course of development, there are lots of power grid component modules which have the nonlinearity characteristic. One obvious example is the solar panel as the system's P-V curve is not linear. People are conventionally using PI control to regulate the voltage and current in the system and then generate the pulse signals for converting DC to AC energy.

The underlying challenge of using such a method is that all these conventional PI controller developments are under one background while all the details/parameters of the power system are given and the controller is developed based on that. Though we are still able to generate the controllers' parameter, it will no longer be accurate as the system has a lot of nonlinearity. All those classical control technique will be inaccurate as we are unable to obtain the accurate system's information or following the information of the system. However, many modern control techniques can address these challenges effectively.

As mentioned in the introduction chapter, there are several adaptive control methods used. They are: gain scheduling, model reference adaptive control, and self-turning regulation. Model reference adaptive control is used in this dissertation work. It is going to improve the conversion ratio of the power conversion system. The beauty of model reference adaptive control is the controller can modify the characteristic of the plant by only tuning the controller's parameters based on the errors between the state variables and the system output. The properties of the plant, under the effect of the controller, approaches to the properties of the reference model. Usually, the reference model is predefined. The controller's parameters are determined based on the output error signal and the tuning parameter's error. The underlying control principle guarantees that the converged parameters making the entire system converges to zero, in other word, the

system's output error and controller parameters' error are asymptotically converging to zero and therefore it 'learned' the characteristic from the reference model [33].

This dissertation develops a hierarchical adaptive control for the MPPT control algorithm that utilizes the ripple correlation control as the first level and model reference adaptive control as the second level. Its ultimate goal is to eliminate or mitigate the transient oscillation and approach the maximum power point efficiently. The specific configuration of the proposed system will be discussed in the following chapters. It also contains the feed forward loop, which is used to obtain the error signal to tune the characteristic of the plant to the reference model. As a result, the entire photovoltaic power conversion system are improved to eliminate any potential transient oscillations in the system's output voltage. Transient oscillations in the system's output voltage can result after the duty cycle has been updated to account for rapidly changing environmental conditions. To prevent the plant from displaying such oscillations, a critically damped system is implemented as the reference model. In the adaptive control, the error from the output response, which is the error signal of the system's response and the reference model's output response, and the signals from the difference of the controller's parameters change. Properly tuning the controller parameters enables the output of the plant to match the output of the reference model, at which point the error converges to zero asymptotically and the maximum power is achieved.

3.0 SYSTEM MODELING

3.1 SOLAR PANEL CONVERSION SYSTEM DEVELOPMENT

3.1.1 SYSTEM DESCRIPTION

1. Solar characteristic

Learning the characteristics of the Sun will better allow us to understand the time constant of the Sun's variation in solar radiation. As a result, the time constants of the controller can be determined. The reason is that if the time constant of the Sun is on the order of second, it means that the Sun's irradiation is changing every several seconds. For a simple example, if the solar radiation is changing every 5 seconds [34], that means in 5 seconds the corresponding power tracking problem should be solved and the maximum power point should be tracked, otherwise, the operating point will move on while the controller is still stuck in the original phase. Based on the literature review and public data on solar irradiance information, the Sun's time constant is on the order of seconds [34]. That is why the sampling period of either observatory or research lab is always five seconds for the smallest sampling unit. Based on the given finding of the Sun's time constant, this will also add a filter on the ripple component of the voltage and current in the solar panel. As a result, it is equivalent to adding a band-pass filter to the voltage and current of the solar panel's outputs such that the DC component in the voltage and the current values are eliminated and also the high frequency component due to the change of the Sun.

In conclusion, the given ripple component of the voltage and current in the RCC algorithm is within a stable frequency window. The information in these ripple components are steady enough to determine the corresponding duty cycle, which will be fed into the conversion system in the solar panel.

2. PV characteristics

In Figure 2 and Figure 4, they present the voltage-current characteristics of photovoltaic systems under various levels of solar insolation and the solar panel's working temperatures. The maximum power point occurs at certain points which are highlighted in these figures. As shown in the figures, the curves may have different shapes when the external temperature or solar radiation are numerous. To find the maximum power point, the nominal voltage or current value needs to be found, which is denoted as $v_m m$ or i_m.

In Figure 3, it shows the underlying structure of photovoltaic system. It is equivalent to the current source parallel connected to two diodes. One photovoltaic module is constructed by connecting the solar cells in parallels or in series. In this analysis, it is recommended connecting them in series as it is easier to generate the voltage and current magnitudes closed to the load. Each solar panel is designed to bypass a connection in case one panel is out of use in practice. Whenever there is certain dysfunction or anything happen to certain panel, the bypass circuit can be activated to disconnect the panel from the entire system. As shown in Figure 3, it shows the single solar cell's model. It consists of the current source, labelled as I_{ph}, and the paralleled connected with two diodes. In some model, it uses one single diode model for representing the solar cell. We can regulate the voltage or current of the solar panel using a dc-to-dc converter

interfaced with an MPPT controller to deliver the maximum allowable power [35, 36]. The underlying mathematical equations of representing solar panel are shown in the (1)

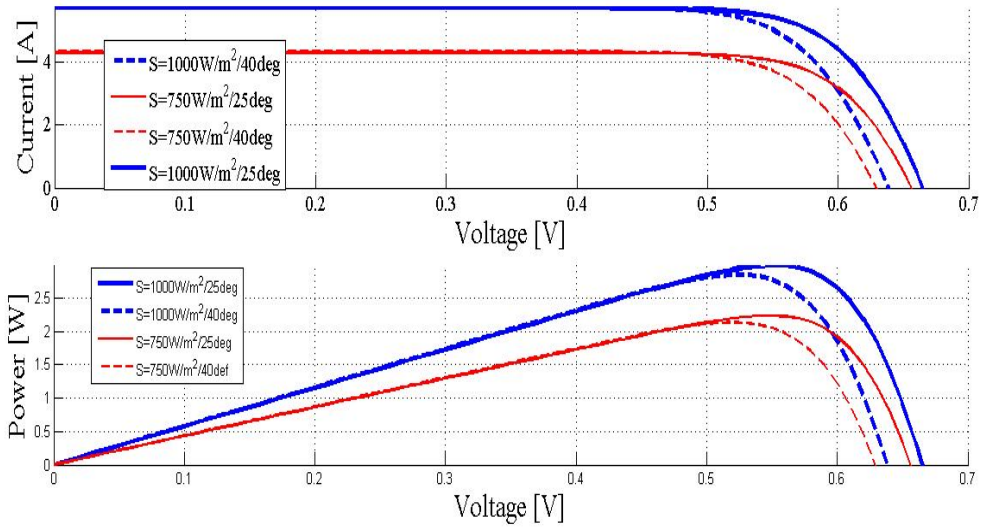

Figure 2: The characteristic of the solar panel under different environment situations.

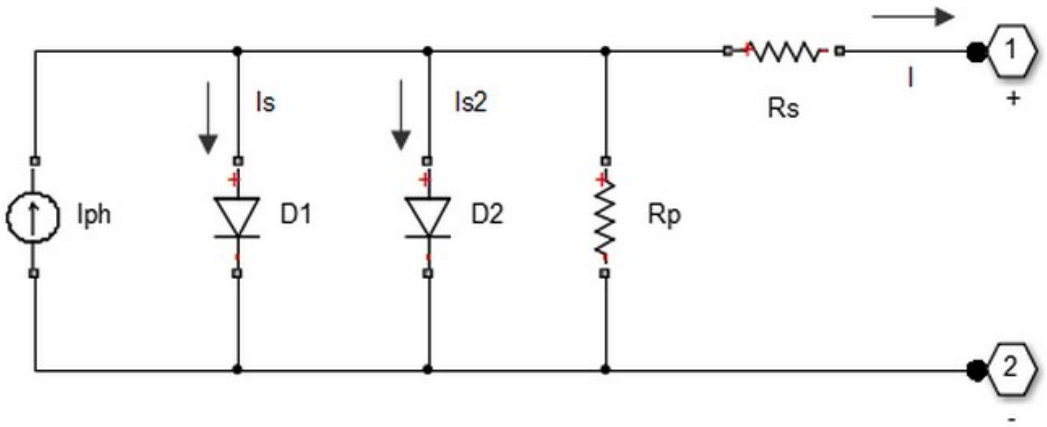

Figure 3: PV model's circuit topology in Simulink.

In the equation (1) aforementioned, I_{ph} is the solar induced current and I_s is the saturation current of the first diode. I_{s2} is the saturation current of the second. V_t is the thermal voltage in the equation. *N* is the quality factor of the first diode and N_2 is the quality factor of the second

diode. *V* is the voltage across the solar cell electrical ports. All these information can also be found in the solar cell in Matlab Simulink module.

$$\mathrm{I} = I_{ph} - I_s \times \left(e^{(V+I\times R_I)/(N\times V_t)} - 1\right) - I_{s2} \times \left(e^{\frac{V+I\times R_s}{N_2\times V_t}} - 1\right) - \frac{V + I \times R_s}{R_p} \qquad (1)$$

Figure 3 shows a symbolic representation of the solar panel's configuration, integrated with the MPPT controller and the converter. As we see this figure from left to the right, the energy flow starts from the very left to the right. On the left, the solar panel is exposed to the sunshine which varies all the time. The changing environment forces the characteristics of the solar panels' P-V curves to change all the time. The MPPT algorithm is utilized when it extracts the current and voltage component through the high pass filter. Therefore the high frequency components from the solar panel's output are used to determine whether we should add or subtract some magnitude of voltage/current to the system and change the operating point of the system. The MPPT's output is the duty cycle and it will control the converter's voltage output.

Depending on the application, other power converter topologies may be used in place of the boost converter. In the boost converter system, shown in the following figure, the MPPT controller senses the voltage and current of the solar panel and yields the duty cycle to the switching transistor S. Therefore the duty cycle of the transistor is related to the array voltage through:

$$v_{pv} = i_{pv} R_O (1-d)^2 . \qquad (2)$$

Where V_{pV} and I_{pV} are the solar panel's voltage and current, respectively. And R_O is the load resistance. Both the array voltage and current consist of the average term (DC term) as well as the ripple term, which is caused by the switching frequency in the converter. The goal then is to

design a controller that continually calculates the optimal value of the duty cycle so that V_{pv} tracks V_M and therefore obtains the maximum power point.

3. Converter Dynamics

The equation (2) provides the foundation for conventional MPPT algorithm used to compute the converter's duty cycle in the steady states. However, to optimize transient response, the MPPT control must consider the dynamics between the duty cycle and array voltage. Since transient oscillations are undesirable and can lead to inefficient operation and waste energy, the MPPT control needs to eliminate such transient oscillations in the array. Voltage output after the duty cycle is updated to account for changing environmental conditions. A detailed dynamic model of the boost converter can be found in [28]. To simplify the analysis of the system's transient response, we consider a small equivalent circuit. A resistor R is used to model the solar array with a small signal array voltage and the small signal array current across its terminals.

We can now derive the transfer function from the control signal to the array voltage output in small signal operation around an operating point. This transfer function is characterized by the dynamics of the system. It should be noted that in the dynamic model there is load in the boost converter as battery storage. The energy storage usually stores the energy and its application can range from microgrid to an individual, residential use of solar panel on the roof. Such circuit topology will change the value of v_{pv} in equation (1) and move the operating point in the steady-state response. This will have little effect on system's frequency response for the range of frequencies near the natural frequency. As a result, resonances or under-dampened oscillations will not be observed in the output response of the system.

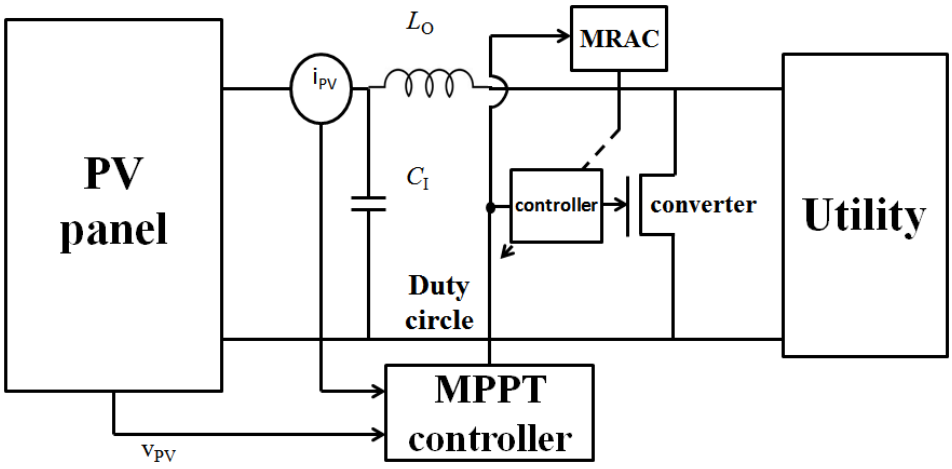

Figure 4: The configuration of the solar panel attached to load.

In Figure 4, it shows that on the right hand side, there has the potential load in the circuit, which can be either a battery, a resistive load, or a utility power grid. Typically there is a DC power link on the right hand side between the power converter and the load side. The purpose of this DC link is to maintain the constant value of the voltage output. The dynamic response from the battery storage will be ignored and our focus will be on the relationship between the changes of duty cycle to the array voltage in small signal operation.

Here is the small signal circuit of the system shown in the Figure 5. Here we insert certain disturbance signals to the equation and then we are able to obtain the small signal circuit of the system and the internal relationship/dynamics is achieved from Figure 5:

And here is the relationship in the frequency domain:

$$\frac{\hat{v}_{PV}(s)}{R_I} + s\hat{v}_{PV}(s)C_I = \frac{f'(D)\hat{d}(s) - \hat{v}_{PV}(s)}{sL_O}. \quad (3)$$

and s is the Laplace operator and $\hat{d}$ represents the small signal variation around the converter's duty cycle D at the operating point.

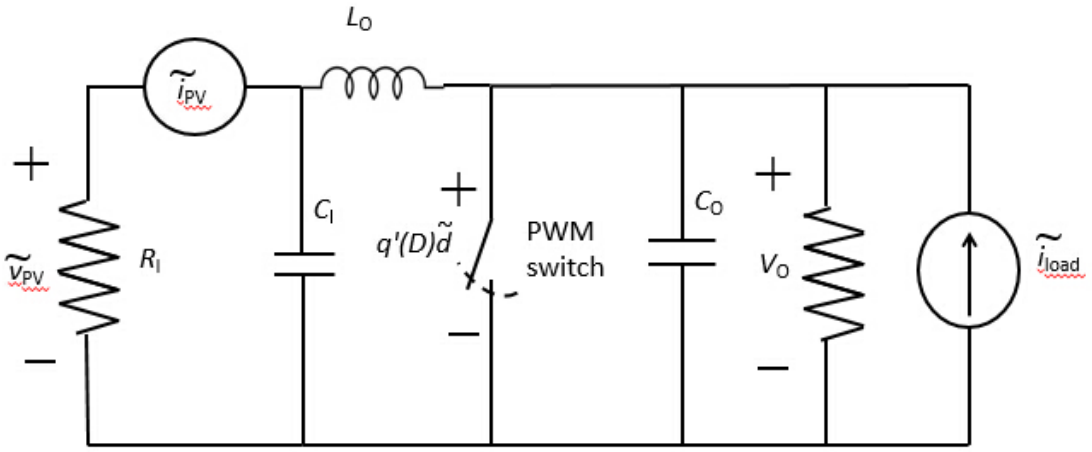

Figure 5: Small signal circuit of the PV conversion system.

On the left hand side of the system, the resistor, R_I represents as the linearized solar panel at certain operating point of the solar panel. The middle part in the circuit is the power conversion system where the voltage magnitude is tuned to the nominal maximum power point voltage. On the right hand side, the current source is representing the load. The load can be either represent as power grid or certain resistive load. Reorganize equation (3) above, the transfer function between the changes of duty cycle to the change of voltage output is shown in below:

$$\frac{\hat{v}_{PV}(s)}{\hat{d}(s)} = \frac{f'(D)}{L_O C_I s^2 + \frac{L_O}{R_I} s + 1}. \quad (4)$$

As shown in the equation above, it is known that $f(D)$ is equal to the expression that:

$$f(D) = (1 - D)V_o. \quad (5)$$

And V is the steady dc output voltage of the boost converter. This relationship indicates that the dc steady-state relationship between $f(D)$ and Vo is unaffected by the transient switching action. And therefore, the equation of (4) can be reconstructed into the following one:

$$\frac{\hat{v}_{PV}(s)}{\hat{d}(s)} = \frac{-\frac{V_o}{L_O C_I}}{s^2 + \frac{1}{R_I C_I} s + \frac{1}{L_O C_I}} . \quad (6)$$

The minus sign in equation (6) is an indication that the reverse characteristic relationship between the change of duty cycle and the change of the voltage output from the solar array. In other words, if the duty cycle increases due to the variation of solar irradiance, then the voltage would decrease down to certain extent. And this transfer function is derived from a linearized circuit of the nonlinear system around a signal operating point. The characteristic of the transfer function of the small signal circuit has this critical term in the denominator:

$$s^2 + 2\zeta w_n s + w_n{}^2 . \quad (7)$$

where w_n is the natural frequency and the natural frequency is determined by the electronics elements:$w_n = \sqrt{\frac{1}{L_O C_I}}$ and the damping ratio's formula expression is $\zeta = \frac{1}{2R_I}\sqrt{\frac{L_O}{C_I}}$.

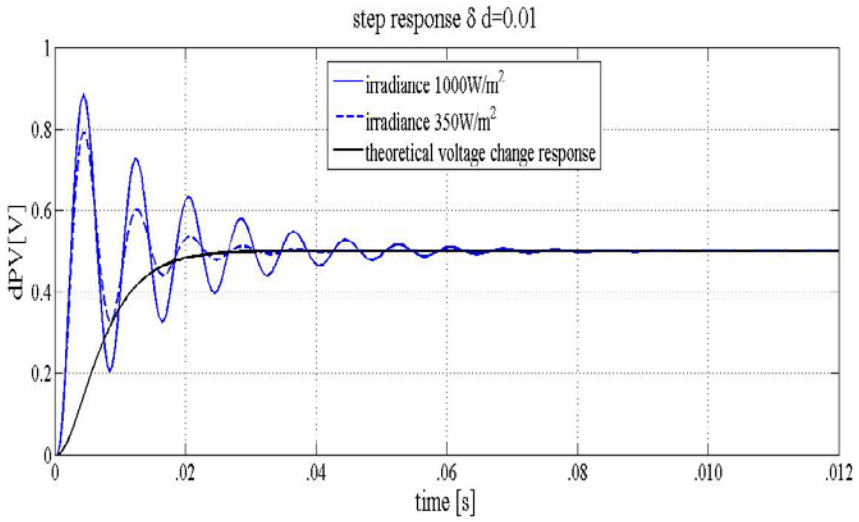

Figure 6: The step response of the small signal circuit.

As shown later, the resistor, which is used to represent the equivalent solar panel in the small signal circuit is the only variable in the system and also determines the damping ratio. In Figure 6, it shows the convergence ratio of the system according to the input duty cycle change has different transient dynamics. We believe that the overall system's response can be optimized as the convergence curve of the voltage lies in the black line and therefore it will not consume any additional energy for searching the optimal operating point. Another thing recalled from the previous section, by using the Ripple Correlation Control (RCC), the duty cycle and the maximum power point found is true maximum power point.

Dynamic characteristic of the linearized solar panel is time-variant and unknown to users when it is functioning on the field. In the classical control, the transient dynamics of system are determined by the damping ratio ζ. When ζ is less than 1, the system has under-damped characteristic and have oscillation during the transient phase. When damping ratio ζ is exactly or around one, then the system will converge to the steady state at the most decent rate without any oscillation. When the damping ratio ζ is larger than 1, then it is called overdamped and it

converges to steady state slower than the system being critical damped. And therefore the goal is to design controller's parameter such that the overall transfer function poses the critical damping characteristic. The contribution of introducing model reference adaptive control is because the resistor R_I cannot be found in the working condition with various solar irradiance. And we need to tune the controller in the solar panel and as a result it has the critical damped characteristic anyway.

As seen in the Figure 7, it is the characteristic of current and voltage of the solar panel. The tangent line represents the linear relationship of the voltage and current and therefore the slope represents the equivalent resistor in the small signal modeling. The slope of that tangent lines is unknown in the most of cases and we use ripple correlation control to find the maximum power point in the system.

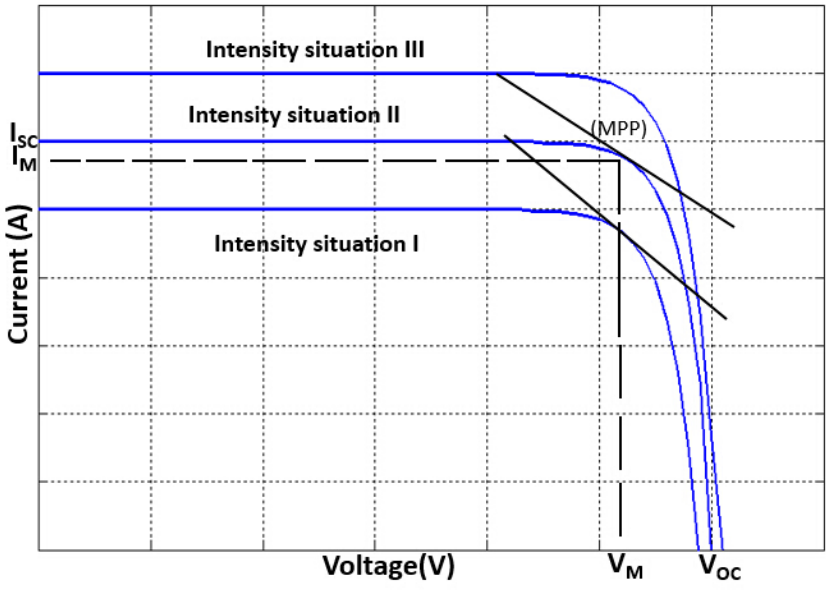

Figure 7: PV model's circuit slope at MPP in I-V curve.

And the analytical relationship of determining value of this resistor can be approximately written as the following equation. And the ripple correlation control is to determine the optimal duty cycle with the value of resistor changing. The details of ripple correlation control (RCC) will be introduced and discussed in the following section.

$$\frac{1}{R_I} \cong -\frac{\Delta I}{\Delta V} \tag{8}$$

4. Ripple Correlation Control

As mentioned earlier, there is a ripple correlation control in this hierarchical control structure, which is mainly used to find the optimal duty cycle under various environmental condition. Ripple correlation control is similar to the algorithm of perturb and observe, however, the major difference between these two methods is that the perturb and observe method is basically using external signal of the voltage and current output to determine the current operating point; while ripple correlation control is using the existing signal from the converter to determine the location of operating point. In another word, P&O algorithm always needs extra energy to produce perturbance even the current voltage value is already around the nominal voltage value corresponding to the maximum power point.

The underlying principle of ripple correlation control is still quite similar to the P&O algorithm, however, by taking advantage of existing ripple components in the voltage and current from the power converter, this algorithm saves a lot of energy used track the maximum power point. This is the major contribution of the RCC algorithm. Here the principle of RCC is formalized in the following. Recalling the output of the voltage and current due to the PWM, it always has decent amount of high frequency components which can be automatically utilized to

complete in the calculation. After equation set (9), there is another flow chart which is commonly used for implementing the RCC algorithm. As indicated in equation set (9), the relative distance from the operating point to the nominal operating point is uncovered. And the control law of the RCC is also revealed:

$$\begin{cases} \frac{dp_{PV}}{dt}\frac{dv_{PV}}{dt} > 0 & when\ V_{PV} < V_{\mathrm{M}} \\ \frac{dp_{PV}}{dt}\frac{dv_{PV}}{dt} < 0 & when\ V_{PV} > V_{\mathrm{M}} \\ \frac{dp_{PV}}{dt}\frac{dv_{PV}}{dt} = 0 & when\ V_{PV} = V_{\mathrm{M}}\,. \end{cases} \tag{9}$$

The control law of the RCC can be written as following:

$$\frac{d\,d(t)}{dt} = \mathrm{k}\frac{dp_{PV}}{dt}\frac{dv_{PV}}{dt}\,. \tag{10}$$

In (10), k is negative constant number for the controller construction. This control law can be qualitatively described as follows in English: when the optimal maximum power point lies on the right to the current operating point, the product of ripple component of power and voltage is larger than zero. When the optimal maximum power point lies on the left to the current operating point, the product of ripple component of power and voltage is small than zero. When the product is equal to zero, which indicates that the current system operating point is the nominal maximum power point. So accordingly a small voltage incremental step along the positive or negative direction is added to the voltage and it drives to approach to the nominal voltage. Proceeding to the aforementioned statement, voltage value will increase or decrease based on the concerning operating point.

In addition to steady-state analysis, it is also very critical to consider the transient response of the boost converter system. So that the controller converges to the theoretical MPP with minimal oscillation and therefore the loss of energy is also minimized. In the following figure, it shows the transient oscillation when there is small change in the duty cycle, which is the result of

external environment change. Such that duty cycle change may lead to voltage change and shows underdamping oscillation in the transient phase. The simulation is conducted in the Matlab. In the power conversion system, there are quite many oscillations within the system, which are generated within the boost converter. Rather than eliminate these ripples by using the filters, people develop the algorithm by utilizing these ripple components to detect the corresponding duty cycle of the conversion system. And therefore, not surprisingly, name this method ripple correlation control. The product of the ripple components of voltage and current is utilized to define the relative location of the current operating point to the nominal operating point. And the product of ripple components multiples to the certain gain would achieve the new duty cycle of the conversion system.

To make sure two algorithms decoupling with each other, the adaptive control, which will be discussed in the following section is restrained by the time constant of the controller. However, we are unable to guarantee that the ripple correlation control has certain time delay, which is discrepancy to the time constant of the MRAC. To make sure it will achieve such goal, a bandpass filter is introduced into the ripple correlation control and therefore such dynamics, in term of oscillation, will be maintained the useful part and get rid of the noise. And therefore with the bandpass frequency ranges is also controlled by mean of the design of the filter, the cutoff frequency. We are able to guarantee, regardless of the solar irradiance’s time constant, the system is stable to function.

The following figure shows the entire system. Here is to present the brief procedure of designing filters. It is a proven technology and has lots of specific application in industrial. The filter is using Butterworth type of bandpass filter and its center frequency is 10 times difference to the cutoff frequency of the MRAC. The bandwidth of the bandpass filter is and therefore, it

has sufficient space to maintain the dynamics of the system. And therefore here is the specifications for the filter. The goal of work here is to provide instruction of how to building filters without considering practical configuration of the filters, which may interface with the boost converter.

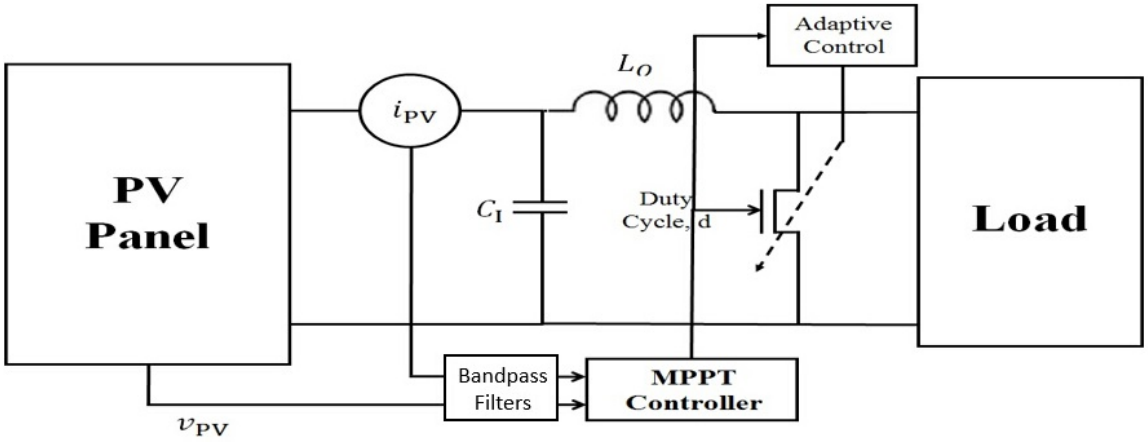

Figure 8: PV model's decoupled control algorithms.

There are three types of filters typically used for the filter design. In general, there also involves some tradeoff between different types of filters. And in this figure, Butterworth filter would be used for designing the filter. It involves sharp cutoff frequency trend and small ripple components in the band pass frequency range. The relationship between the cutoff frequencies versus the time constant of the system bears the following equation:

$$f_{\text{cuttoff}} = \frac{1}{2 \times \pi \times \tau}. \tag{11}$$

Although we do have the time constant of the solar irradiance, which is according to the national solar irradiance record. The data sheet shows that the irradiance is measured every five second and we are confident to indicate that the sampling rate for recording solar irradiance is in

the order of second. It has confidence that the solar irradiance's change will be slower than unit of second, for instance during the overcast or shinny day where the solar irradiance remains constant or changes slowly. From the recording history of the solar irradiance, the cutoff frequency of solar irradiance is in the frequency range of 0~0.0318 Hz. We assume that the time constant of the RCC will be slowly enough, considering the slow change of the irradiance. And therefore, we need to design the bandpass filter covers this specific range of frequency. Meanwhile, the range of the MRAC control algorithm should be faster and there has a sufficient discrepancy between two sections of frequencies range for controller. The cutoff frequency of the MRAC should be larger than 0.5 Hz and the choice of the cutoff frequency is determined by the 0.0318 Hz. And therefore we are able to find the time constant of the MRAC should be at most 0.316 sec. By designing these two time constants for the controllers, it provides sufficient margins between two controllers and also it fits the logic of the reality. As the solar irradiance changes slowly, the adaptive control tunes the system immediately and it damps the oscillation and exhibits the system with critical damping characteristic.

For the future research purpose, as it showed in previous literature that the implementation of the RCC usually is in analogy system and with the development of implementation in digital system, it is going to be able to integrate the digital filter with the digital RCC into one system. Following is the basic procedure for designing filter [37-39].

1). we need to determine the type of the filter, the cutoff frequency and the ripple component within the system.

It involves many consideration for the system. The system frequency gap between the bandpass and cutoff frequency should be well designed otherwise, the potential increase of the cost for the filter is associated. Moreover, there are three basic types of the filters: Butterworth,

Chebyshev and Elliptic type of filters. As shown in , the choice of the filter depends on your practical need.

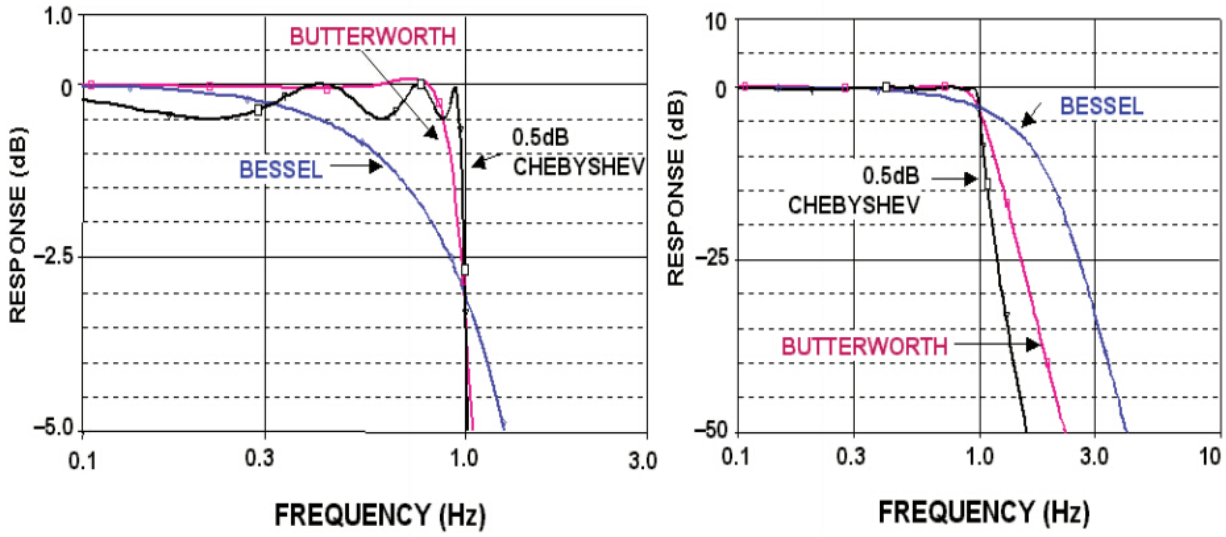

Figure 9: Three types of filters' Bode plots in comparison.

2). The generic model for the bandpass filter is in the following form. And the corresponding values of the system is inserted accordingly:

$$|H_c(j\Omega)|^2 = \frac{1}{1+(\Omega/\Omega_c)^{2N}}. \qquad (12)$$

3). The designed filter is in the analog form and then convert it to the digital form of the filter by mean of bilinear transformation. Since the ripple correlation control is also able to design and implement in the digital domain. And therefore it is useful to utilize such transformation equation to switch the filter from digital domain to analog domain.

5. MRAC Algorithm

MRAC is initialized as Model Reference Adaptive Control. In the previous section, the advantage of MRAC or adaptive control is briefly discussed. In the RCC, the duty cycle is always changing a little bit to find the maximum power point. As shown in figure, transient response has quite many oscillation, which highly depends on the damping ratio. We need to change the overall system's damping ratio to be close to 1 and therefore it will not occur oscillations in the systems.

The basic idea of MRAC is to design an adaptive controller so that the response of the controlled plant remains close to the response of a reference model. This reference model carries desired dynamics character, despite the uncertainties and variations during the plant parameters. The proposed MRAC structure is shown in the figure below. In this figure, the input to the system is deviation of duty cycle, achieved by the duty cycle at the current sampling time and one sampling period before. The plant box represents the small signal model derived based on the linearized converter system. And there is one changing variable in that box, which is equivalently represented by the resistor. The object in this subsection is to design an adaptive controller so that the response of the controlled plant remains close to the response of a reference model with desired dynamics. Assuming the transfer function of the system can be represented as following and denoting as $G_p(s)$. The letter p stands for the plant system of small signal circuit model. And the $u(t)$ is the input to the plant model and also the controller's output. $y(t)$ is the output of the plant model:

$$G_p(t) = \frac{y_p(s)}{u_p(s)} = \frac{k_p}{s^2 + a_p s + b_p}. \tag{13}$$

The parameters in equation (13) can be implied from the small signal circuit of the boost converter. The equations of the parameters are related to the electronic component in the boost converter and it shows the specific values of these parameters in Table 2. The reference model is designed by users and the transfer function of the reference model having the similar representation as the transfer function of the plant model:

$$G_{\mathrm{m}}(s) = \frac{y_{\mathrm{m}}(s)}{r(s)} = \frac{k_{\mathrm{m}}}{s^2 + a_{\mathrm{m}}s + b_{\mathrm{m}}}. \tag{14}$$

The value of a_{m}, b_{m} are determined according to equation (13) and (14). Since the parameters in equation (14) are given and therefore the reference model system needs to determined. These parameters are to be positive. The parameters of reference model are preferred to be more close to the plant model. Analytically, b_{m} should be the same as b_{p} because this is the square of the natural frequency of the plant model and there is no need to make a modification, considering the energy used in the controller. Four steps are required to derive the adaptive law for controller's parameter in MRAC:

i). Choosing the controller structure;

ii). Finding state space equations for the controlled plant and the reference model;

iii). Constructing the error equations from the reference model and plant model's state space equations;

iv). Deriving the adaptive control law by constructing the Lyapunov function.

Controller's Structure: the controller's structure is shown in the following expression and in this equation, r is the reference signal to the system meaning that it is to design the system's output having the same dynamics and magnitude of the reference signal, r. u_p is the controller signal and y_p is the output signal of the system.:

$$u_p = \theta_0 r + \theta_1 \frac{1}{s+\lambda} u_p + \theta_2 \frac{1}{s+\lambda} y_p + \theta_3 y_p \,. \tag{15}$$

It is defined that the series of parameter: $\theta = [\theta_0, \theta_1, \theta_2, \theta_3]^T$ and the controller parameters are the goal in the MRAC need to be determined. Two sets of formula equations are defined as:

$$\begin{aligned} w_1 &= \frac{1}{s+\lambda} u_p \\ w_2 &= \frac{1}{s+\lambda} y_p \,. \end{aligned} \tag{16}$$

In the equations (16), s represents the Laplace operator. The signal obtained in the converter, u_p andy_p, are carrying noises from the boost converter. To simplify the equation expression, another vector is introduced as$w = [r, w_1, w_2, y_p]^T$. And therefore, a proper simple filter is added to eliminate the undesired frequency component and also guarantee that the system is stable. It is shown in the literature [40-42] that the controller structure in equation (16) is sufficient to achieve the control objective: it is possible to make the transfer function from r to y_p equal to the transfer function of desired reference model, namely that $y_p(s)/r(s)$ equals to $y_m(s)/r(s)$when the nominal controller parameters are meet: $\theta^* = [\theta_0^*, \theta_1^*, \theta_2^*, \theta_3^*]^T$ and each parameters are found as follows. These parameters can be found by equating the reference model

transfer function to be the same as the plant model transfer function. By having these parameters value, we are able to express the state space expression of the system. Moreover, these values are acquirable because the reference model is designed and the given plant model is known at prior.

$$\theta_0^* = \frac{k_m}{k_p}$$

$$\theta_1^* = a_p - a_m$$

$$\theta_2^* = \frac{(a_p - a_m)(-\lambda^2 + \lambda a_p - b_p)}{k_p} \tag{17}$$

$$\theta_3^* = \frac{b_p - b_m + (a_p - a_p)(\lambda - a_p)}{k_p}.$$

State-space Expressions of the Controlled Plant and the Reference Model: Let $[A_p,\ B_p,\ C_p]$ be a minimal realization of the plant $G_p(s)$:

$$\dot{x}_p = A_p x_p + B_p u_p$$

$$y_p = C_p x_p. \tag{18}$$

In the above equations, $x_p$is a 2-D state vector. By replacing the controller's expression, shown in the above, then the minimal realization of the plant can be reconstructed as the following:

$$\dot{x}_{pn} = A_{pn} x_{pn} + B_{pn}\theta_0^* r + B_{pn}(B_{pn} - \theta^{*T} w)$$

$$y_p = C_{pn} x_{pn}. \tag{19}$$

In the (19), x_{pn} is an extended state space vector, which also includes the state variable w_1 and w_2. And three matrix A_{pn}, B_{pn} and C_{pn} are defined as:

$$A_{pn} \equiv \begin{bmatrix} A_p + \theta_3^* B_p C_p & \theta_1^* B_p & \theta_2^* B_p \\ \theta_3^* C_p & -\lambda + \theta_1^* & \theta_2^* \\ C_p & 0 & -\lambda \end{bmatrix}$$

$$B_{pn} \equiv \begin{bmatrix} B_p \\ 1 \\ 0 \end{bmatrix} \tag{20}$$

$$C_{pn} \equiv [C_p \quad 0 \quad 0].$$

Since the controller equation expression indicates that $u_p = \theta^{*T} w$ and therefore equation (19) is re-organized into the following equation set:

$$\begin{aligned} \dot{x}_{pn} &= A_{pn} x_{pn} + \theta_0^* B_{pn} r \\ y_p &= C_{pn} x_{pn}. \end{aligned} \tag{21}$$

So when the controller's parameters are close to the nominal controller parameter, the condition that $y_p(s)/r(s) = y_m(s)/r(s)$ is satisfied. And therefore, $\{A_{pn}, \theta_0^* B_{pn}, C_{pn}\}$ should be a realization of the reference model. In other words, the reference model can be realized by the following state space equation:

$$\begin{aligned} \dot{x}_{mn} &= A_{mn} x_{mn} + \theta_0^* B_{mn} r \\ y_m &= C_{mn} x_{mn}. \end{aligned} \tag{22}$$

Error Equations: By subtracting the reference model's state-space equation (22) from the plant's state-space equation (21), the error between these two systems is also in the form of state-space equation. By defining e, e_0 and $\tilde{\theta}$. These three are the state error, tracking error (output error) and controller parameter error, respectively:

$$\begin{aligned} e &\equiv x_{pn} - x_{mn} \\ e_0 &\equiv y_p - y_m \\ \tilde{\theta} &\equiv \theta - \theta^*. \end{aligned} \tag{23}$$

In finding the adaptive law for the controller by mean of Lyapunov function, the input-output transfer of a state-error equation should be strictly positive real (SPR) [43, 44]. Nevertheless, the transfer function of the realization $\{A_{pn}, B_{pn}, C_{pn}\}$ is not strictly positive real, because $C_{pn}(sI - A_{pn})^{-1}B_{pn}$ equals to $G_m(s)/\theta_0^*$ according to the state space equation in (23) and the relative degree of is 2. And these information indicates that is not SPR.

To cope with the difficulty as mentioned above, the identity $(s+g)(s+g)^{-1} = I$ is multiplied on both sides of the equation in (23) and the equation is rewritten as follows:

$$\begin{aligned} \dot{e} &= A_{pn}e + B_{pn}\{(s+g)(u_g - \theta^{*T}\phi)\} \\ &= A_{pn}e + B_{pn}\{(s+g)\tilde{\theta}^T\phi\} \\ &= e_0 = C_{pn}e\,. \end{aligned} \tag{24}$$

In equation (25), and u_g and ϕ are introduced and their expressions are:

$$\begin{aligned} u_g &\equiv \frac{1}{s+g}u_p \\ \phi &\equiv \frac{1}{s+g}w\,. \end{aligned} \tag{25}$$

The term $s+g$ increase the degree of the numerator to make the relative degree of transfer function equal to one. And then the realization of $\{A_{pn}^o, B_{pn}^o, C_{pn}^o\}$ is SPR. The denotation is different to the original sets of matrix and the new matrix with integrating the identity equation. Since $u_g = \theta^T\phi$, the controller expression can be written as:

$$\begin{aligned} u_p &= (s+g)u_g \\ &= \dot{\theta}^T\phi + \theta^T\dot{\phi} + g\theta^T\phi \\ &= \dot{\theta}^T\phi + \theta^T(\dot{\phi} + g\phi) \\ &= \dot{\theta}^T\phi + \theta^T w. \end{aligned} \tag{26}$$

And now introduce the following equation. This equation is critical because we are able to express the error signal in form of variables and as a result, as the ultimate goal of adaptive control, we are able to make error signal to approach to zero.

$$\bar{e} = e - B_{pn}\tilde{\theta}^T\phi . \tag{27}$$

Then, it can be derived that:

$$\begin{aligned} \dot{\bar{e}} &= A_{pn}\bar{e} + \left(A_{pn}B_{pn} + gB_{pn}\right)\tilde{\theta}^T\phi \\ e_0 &= C_{pn}\bar{e} + C_{pn}B_{pn}\tilde{\theta}^T\phi . \end{aligned} \tag{28}$$

In the equation (29), define a new matrix B_1 and it is equal to $A_{pn}B_{pn} + gB_{pn}$ and noting that $C_{pn}B_{pn}$ equals to zero. The reason underlying that is because the relative degree of the reference model is two. And the leading coefficient is zero for the numerator of $C_{pn}(sI - A_{pn})^{-1}B_{pn}$. The equations (28) become into:

$$\begin{aligned} \dot{\bar{e}} &= A_{pn}\bar{e} + B_1\tilde{\theta}^T\phi \\ e_0 &= C_{pn}\bar{e} . \end{aligned} \tag{29}$$

the above equations achieved are so-called the new state-space equation of error. These two equations are equivalently the same and since they are the same, the realization of $\{A_{pn}, B_{pn}, C_{pn},\}$ has the following transfer function:

$$\begin{aligned} C_{pn}(sI - A_{pn})^{-1}B_1 &= C_{pn}(sI - A_{pn})^{-1}B_{pn}(s+g) \\ &= (s+g)\frac{G_m}{\theta_0^*} \\ &= \frac{k_m}{\theta_0^*} \times \frac{s+g}{s^2 + a_m s + b_m} . \end{aligned} \tag{30}$$

where the positive constant g is chosen to be less than a_m. It can be shown that in the above

equation that this equation is SPR for any g as long as it satisfies the condition that: $0 < g < a_m$

Derivation of the Adaptation Law: the adaptive law for the controller is derived, based on the stability theory of Lyapunov function. A typical trial of constructing a Lyapunov function is in the following form:

$$V(\tilde{\theta}, \bar{e}) = \frac{\bar{e}^T P \bar{e}}{2} + \frac{\tilde{\theta} \Gamma^{-1} \tilde{\theta}}{2}. \tag{31}$$

There are two variables in this Lyapunov function: one is the state error and the other one is the controller's parameter error. In the error Lyapunov function, is an arbitrary symmetric positive definite matrix and P is a symmetric positive definite matrix determined using Meyer-Kalman-Yakubovich Lemma [44, 45].

According to this lemma, since A_{pn} is stable and $\{A_{pn}, B_{pn}, C_{pn},\}$ is a minimal realization of the SPR transfer function in (31). And then according to the lemma, there exists a symmetrical positive definite matrix P, a vector q and a scalar $\upsilon > 0$, such that the following equations are satisfied with any give symmetric positive definite matrix L:

$$\begin{aligned} PA_{pn} + A_{pn}{}^T P &= -qq^T - \upsilon L \\ PB_1 &= C_{pn}^T. \end{aligned} \tag{32}$$

It also need to be noticed that the matrix P in the (29) is also satisfied in (30). The significance of MKY (Meyer-Kalman-Yakubovich) Lemma is that it facilitates to find the derivative of Lyapunov function respect to the variable $\tilde{\theta}$ and $\bar{e}$. The time-derivative of the Lyapunov function along the solution of (27) can be calculate as:

$$\dot{V}(\tilde{\theta}, \bar{e}) = -\frac{1}{2}\bar{e}^T q q^T \bar{e} - \frac{\upsilon}{2}\bar{e}^T L \bar{e} + \bar{e}^T P B_1 \tilde{\theta}^T \phi + \tilde{\theta}^T \Gamma^T \dot{\tilde{\theta}}. \tag{33}$$

since $\bar{e}^T P B_1 = \bar{e}^T C_{pn}^T = e_0$, then we can choose:

$$\dot{\theta} = \dot{\tilde{\theta}} = -\Gamma e_0 \phi \,. \tag{34}$$

Based on equation (32), (31) can be simplified into the following equation:

$$\dot{V}(\tilde{\theta}, \bar{e}) = -\frac{1}{2}\bar{e}^T q q^T \bar{e} - \frac{v}{2}\bar{e}^T L \bar{e} \leq 0 \,. \tag{35}$$

By achieving the result above, that means the Lyapunov is positive definite function and its derivative function of Lyapunov function along the solution is negative definite. And therefore, it is sufficient and necessarily to claim that the errors, which are the controller's parameter error vector and the state error, asymptotically converge to zero. In other words, these variables are both stable and bounded. According to the derivations above, the overall control rule of MRAC are concluded as follows:

$$\begin{cases} \omega_1 = -\lambda\omega_1 + u_p \\ \omega_1 = -\lambda\omega_2 + u_p \\ \phi = -g\phi + \omega, \omega = [r \quad \omega_1 \quad \omega_2 \quad y_p]^T \\ u_p = \theta^T\omega + \dot{\theta}^T\phi = \theta^T\omega - \phi^T\Gamma e_0\phi \\ \dot{\theta} = -\Gamma e_0 \phi. \end{cases} \tag{36}$$

By having the control actions to tune the characteristic of the solar system, it will require some techniques to decouple these two control algorithms together and make sure the computation and signal flow doesn't conflict with each other and eliminate or mitigate the control effort.

As recalling the previous section, the time constant of two control algorithms determines whether it is feasible for two control algorithm to decouple or not. The time constant of the adaptive control, MPPT, is determined by the control matrix. This means that the larger of the control matrix, Γ, the faster of the control response will make. The other level of the control algorithm is the ripple correlation control and it is depending on the time constant of the solar.

By introducing several filters into the system, it can successfully manipulate the time constant of the RCC control.

As implementing in the system, it is introducing two bandpass filters into the system to guarantee that the two control algorithm’s time constant are distant to each other. The following paragraphs are going to discuss the procedure for designing the band pass filters.

4.0 DEVELOPMENT OF MICROGRID STABILITY

Shown in the Figure 10 below, it is the expansion in coupling offshore renewable energy. This system includes variable frequency drive based platforms, and the microgrid theme. The proposed system architecture is provided in Figure 10 utilizing a DC backbone. The directions that many manufacturers of power system equipment are exploring with offshore technologies to harness and transmit electric power provides further encouragement that the proposed research efforts/system architecture is viable [46, 47]. In many literature, it demonstrates the advantage and disadvantages of AC microgrid vs. DC microgrid system. It is obvious that as the rise of solar energy and need of infrastructure for long distance bulk energy transmission, DC microgrid poses many advantages. However, it this specific application, which shall be widely used for offshore wind generators power supply, it is essential to develop the AC microgrid and several issues are to be discussed in the following paragraphs.

The DC renewable generators with power electronic converters and motor drives can be treated as constant power loads (CPL). For the case of a motor drive, the inverter drives the motor and tightly regulates the speed as approaching the constant speed as required. Assuming the relationship between the torque and speed in the motor drives is linear. Then the motor torque will remain constant in the constant power consumption by the motor. In the CPL, it is easy to observe that the instantaneous value of impedance is positive: as the ratio between the voltage and current is positive. However, the incremental impedance is always negative, if you

observe the V-I curve of the constant power load it is easy to find that dV/dI<0. And in the literature [17], the latter is referred as negative incremental impedance instability [25].

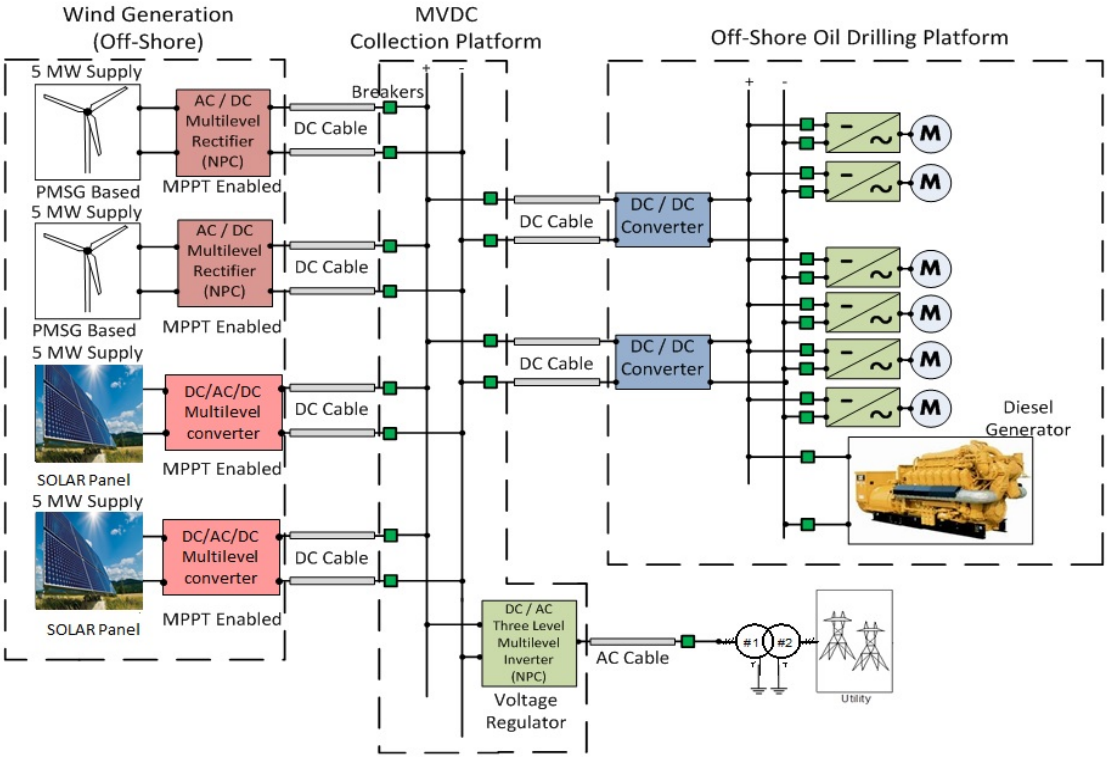

Figure 10: Local offshore wind power supplying power to offshore production platform.

CPL induced instability or oscillations can be resolved by modifying the DC system's hardware structure, by adding resistors, filters, or energy storage elements. However, approaches based on feedback control can offer more practical and efficient solutions. In addition to linear controllers featured by simple architectures and designs, many research teams have chosen nonlinear based control approaches to stabilize CPL scenarios to avoid limitations of linearization (operating closely to the system equilibrium point) and large-signal stability is guaranteed [32, 48-50]. The primary nonlinear approaches include the use of Lyapunov-based design, hysteresis control, nonlinear passivity-based techniques, and boundary control. However, some of the disadvantages

of these techniques include the use of proportional-derivative (PD) controllers which can be sensitive to noise, current and voltage transient overshoots, and difficulty with implementation.

In order to transmit the power from the DC source side to the CPL load side, it uses the duty cycle of the power converter for tuning the amount of power. The figure below depicts the energy flow diagram of the system where the network node collects the voltage, current data is directed to the centralized server where it calculates the duty cycle, and fed the calculated ones to the local converter through telecommunication system. Such configuration is realized by using the Simulink interfacing with C language in the simulation environment. However, the results obtained from the simulation are unstable and the underlying reason is because of the time delay effect in the system.

4.1 FUNDAMENTALS OF BIDIRECTIONAL DC/DC CONVERTERS AND SYSTEM DEVELOPMENT.

The dual active bridge DC/DC converter shown in Figure 11 was first proposed in [51, 52]. The converter topology has grown in popularity as demand in bidirectional power flow capability has increased in research pursuits such as battery charger applications for electric vehicles. Research teams have devised new control techniques for improving system efficiencies [48-52] and using state of the art semiconductor devices for high frequency operation of the topology [53-57]. Research efforts have been primarily centered upon low power applications.

In this work, dual active bridge is used as the interface between two medium voltage DC buses. As shown in the figure below:

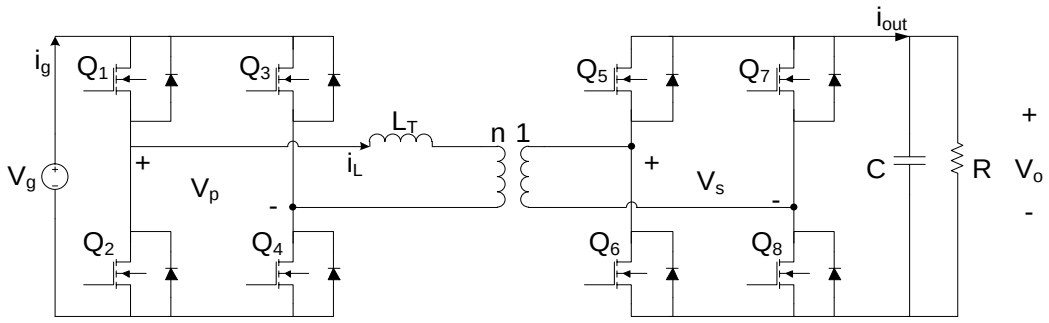

Figure 11: Dual active bridge bidirectional DC/DC converter.

As the actual need for the system's configuration, the power flow is going to flow in either ways according to the different systems' requirement. The most notable characteristic associated with this topology is the phase delay, ϕ , between both bridges, which controls the allowable power flow in the circuit. The relationship between the phase delay and duty cycle, d_h, is described by:

$$\phi = \frac{d_h T_s}{2}. \tag{37}$$

where T_s is the switching period. And by the empirical model of the DC converter, the average of the converter can be generalized into an average inductor current source where the current is implemented as:

$$I_{avg} = \frac{nV_{DC}T_s}{2L_T} d_h(1 - d_h). \tag{38}$$

where V_{DC} is the DC source input voltage, L_T represents transformer leakage inductor and n is the turns ratio of the high frequency transformer[14]. The output voltage as a function of the converter duty cycle and output impedance, Z_{out}, of the converter is described by:

$$V = I_{avg} Z_{out} = \frac{nV_{DC}T_s}{2L_T} d_h(1 - d_h) Z_{out}. \quad (39)$$

If we apply a small perturbation to both the output voltage, $\hat{V}$, and duty cycle, $\hat{d}_h$, of (39) and linearize, the linear small signal transfer function between the output voltage and duty cycle becomes:

$$\frac{\hat{V}}{\hat{d}_h} = \frac{nV_{DC}T_s}{2L_T} d_h(1 - d_h) Z_{out} \equiv K_{DC} Z_{out}. \quad (40)$$

where K_{DC} denotes $nV_{DC}T_s(1-2d_h)/(2L_T)$. Eq. (40) is the plant to be controlled and will be shown to be naturally unstable.

4.2 CONSTANT POWER LOAD MODEL DEVELOPMENT

The following figure, Figure 10, is the key section of the overall power system and will be studied thoroughly in this work [53]. Starting from left to right, the medium voltage DC bus has been replaced with an ideal voltage source (assuming well-regulated DC bus) and a bidirectional DC/DC converter interfaces the medium voltage DC bus with the induction motor inverter. A 7.2 kV rated, single core, XLPE insulated, PVC sheathed, unarmoured cable bridges the power converters and is modeled as a coupled pi circuit as shown [58].

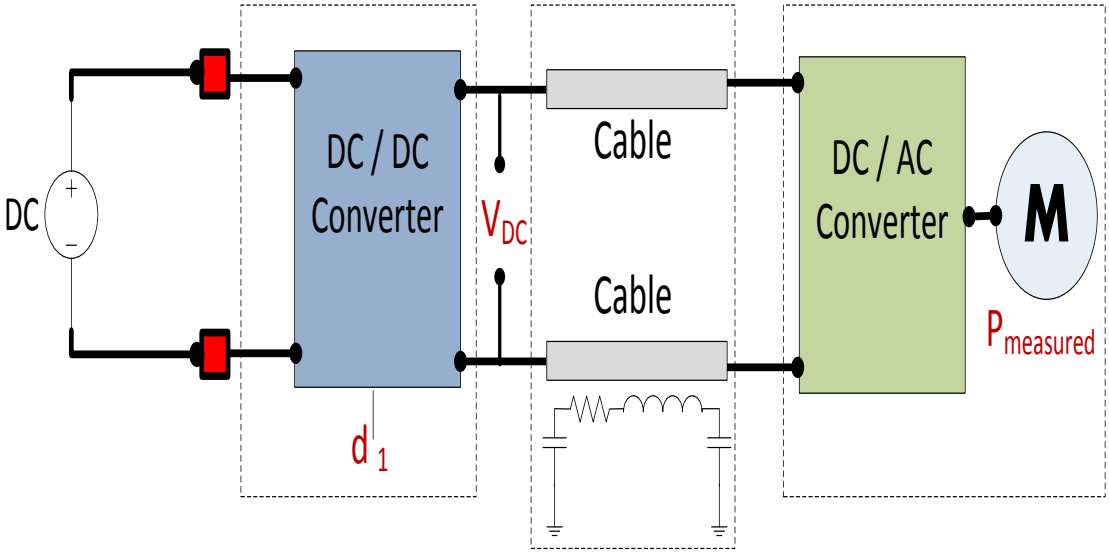

Figure 12: System model under study.

As described in [59,60], a common constant power load is a DC/AC inverter that drives an electric motor and tightly regulates the speed of the machine to be constant. Assuming a linear relationship between torque and speed, for every speed there is one and only one torque. For constant speed, torque will be constant as well as power. Therefore, the motor/inverter combination presents a constant power load characteristic to the DC/DC converter. With the understanding that the average current of the bidirectional DC/DC converter can be described by (2) and assuming that the DC/AC inverter and motor can be approximately represented as a constant power load (whose time constant is much smaller than that of the DC/DC converter), Figure 10 can be simplified to Figure 12.

The output impedance associated with the simplified system model is described by:

$$Z_{out} = \frac{LC_2Ys^2 + (RC_2Y - L)s + (Y - R)}{LC_1C_2Ys^3 + (RC_1C_2Y - LC_1)s^2 + (C_1Y - RC_1 + C_2Y)s - 1} \quad (41)$$

where the circuit parameters are defined in Table 2. The pole-zero placements of the naturally unstable transfer function is found in Figure 17. For higher power applications, the poles and zeros shift further into the unstable region of the complex plane.

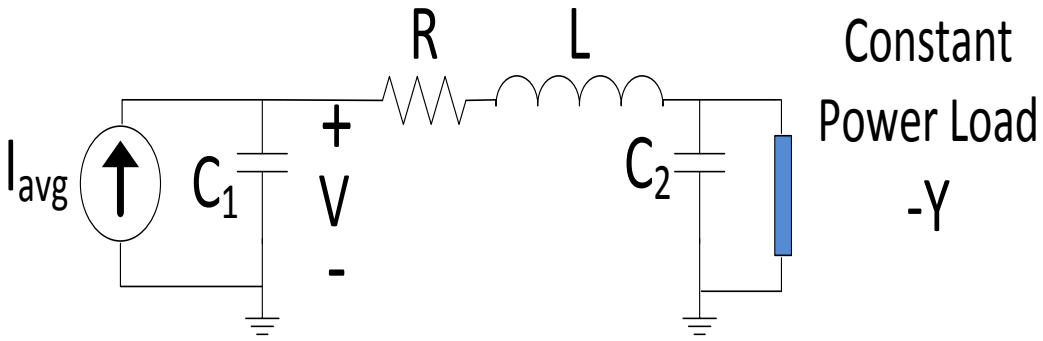

Figure 13: Simplified system model.

Table 2: Cable Parameters.

Parameter	Numerical Quantity
Line Resistance, R	0.0176 Ω/km
Line Inductance, L	0.248 mH/km
Line Capacitance, $2C_{1,2}$	0.923 µF/km
Cable Distance	0.005 km (16 feet)

Based on the previous analysis, the task at hand is to design a controller compensator. Power system engineers are accustomed to using some form of PID controller. The integral (I) control is often used to eliminate steady-state error, while derivative (D) is used to control and improve stability and system damping, This section will first show that the proportional derivative (PD) controller cannot achieve satisfactory steady-state performance and dynamic (e.g. stable) response at the same time. Then the principles of model reference control (MRC) are used to stabilize the system.

To appreciate the damping control effect of a PD controller, we first consider a simplified second-order model of the plant. Because the distance between the DC/DC converter and motor inverter is short (application being on an offshore platform), the cable can be approximated with a line inductance in series (Figure 13) [54, 55]. Noting the output capacitor of the dual active bridge DC/DC converter, the system model can be approximated as a second-order system with output impedance transfer function described by:

$$\frac{\hat{V}}{\hat{d}_h} = K_{DC} Z_{2,out}(s) = K_{DC} \frac{Ls - Y}{LCs^2 - YCs + 1}. \tag{42}$$

where $Z_{2,out}$ represents the simplified second-order output impedance, the meaning of K_{DC} is the pure gain achieved from the dynamics of the duty cycle to the current input. And the other circuit parameters are defined in Table 2.

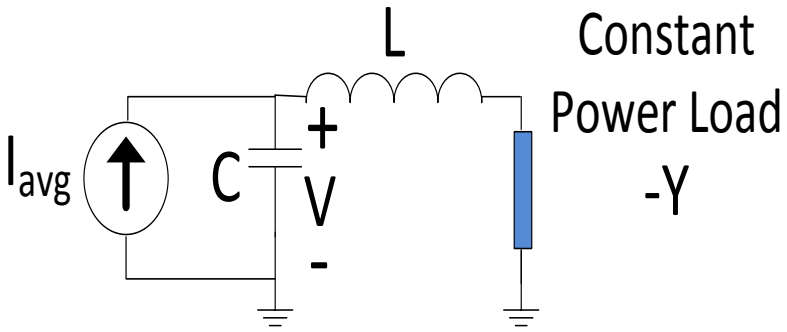

Figure 14: Second-order system model of a simplified system.

The first choice for a controller compensator would be the PD controller [56] because this type of compensation provides a phase lead, which creates a stabilizing effect. Generally for a second-order plant, the derivative (D) part of the PD control can act on the damping component of the closed-loop system and thus stabilize the plant. Figure 15 shows a diagram with PD control in the closed loop.

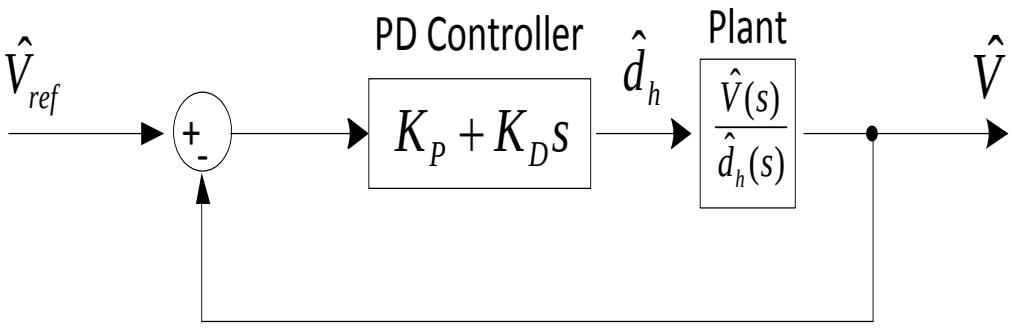

Figure 15: PD control of the plant.

The closed-loop transfer function of the system in Figure 15 can be written as:

$$\frac{\hat{V}(s)}{\hat{V}_{ref}(s)} = \frac{K_{DC}(K_P + K_D s)(Ls - Y)}{As^2 + Bs + (1 - K_{DC}K_P Y)}. \quad (43)$$

In this equation, the parameters A, B can be represented by the components value in the system:

$$A \equiv K_{DC}K_D L + LC$$
$$B \equiv K_{DC}K_P L - K_{DC}K_D Y - YC. \quad (44)$$

And a standard PD compensator of the form $K_P + K_D s$ is used to control the plant in Figure 15 and K_P and K_D are the proportional and derivative gains, respectively. If we express the denominator of (45) as that of a standard second-order system $s^2 + 2\zeta\omega_n s + \omega_n{}^2$ with natural frequency ω_n and damping ratio ς, we can calculate:

$$2\varsigma\omega_n = \frac{K_{DC}K_P L - K_{DC}K_D Y - YC}{K_{DC}K_D L + LC}. \quad (45)$$

$$\omega_n{}^2 = \frac{1 - K_{DC}K_P Y}{K_{DC}K_D L + LC}. \quad (46)$$

A couple of observations can be made on the performance of PD control. First, under the premise of stability, as K_P increases the damping ratio, ς, increases and natural frequency decreases; as K_D increases, the natural frequency, ω_n, and damping ratio decrease. This behavior of PD control is different from the conventional effect of PD control when applied to a stable and minimum-phase plant where, for example, bigger K_D and K_P usually achieve larger damping ratio and higher natural frequency, respectively.

Second, the DC gain of system (47) is:

$$\frac{-K_{DC}K_PY}{1-K_{DC}K_PY} \tag{47}$$

In order for the closed-loop system to be stable, both (45) and (47) need to be greater than 0, i.e., $K_{DC}K_PL - K_{DC}K_PY - YC > 0$ and $K_{DC}K_PY < 1$. However, as $K_{DC}K_PY < 1$, the system's DC gain described by (47) is always negative. Therefore, the PD controller here cannot achieve satisfactory steady-state performance while maintaining system stability.

4.3 TIME DELAY IN THE POWER TRANSMISSION SYSTEM

As derivations and simulations obtained above, the model reference control implemented in the DC power transmission system stabilizes the instability issue caused by the constant power load (CPL). There are several layers of control in the power system: 1). Primary frequency control; 2). Secondary frequency control 3). Tertiary control 4). Generation Rescheduling. These terminologies are declared according to the time constant of the power system. The constant power load stability issue is related to the scope of primary control and when the power

transmission deployment is implemented, it involves secondary frequency control and the time to complete the deployment is around 0.2 second. And therefore it cannot be treated as negligible in the system modeling when the power deployment needs to be performed.

We assume that the power deployment mechanism is centralized power control and in the transmission system the amount of power transmitted through the transmission line is calculated online, according to the relationship between the supply and need. On the supply side, people need to collect the information about source of DC power, such as the weather, the solar irradiance and the wind speed and so on. On the need side, the load consumption profiles need to be collected. Previously, there are three major factors to change/tune the power transmission capability, which are the blade control, the duty cycle in the power converter and power reference of grid connected converter. In this work, the focus is on the control of the duty cycle accorded to the transmitted power amount. Here is the internal mathematical representation of the converter system regulated through the power converter. As shown in equation (48), the variation of duty cycle is going to change the amount of power transmitted:

$$P = \frac{nV_H V_L T_s}{2L_T} d_h (1 - d_h). \tag{48}$$

And in this equation, P is the power amount, n is the number of submodules, V subscripted as H and L are the voltage magnitude on the two side of transmission line. L_T is the leakage inductor in the converter. The value of this leakage inductor is related to the transmission capability. In the analysis model, high end voltage is 5000V and low end voltage is 1000V, respectively. The period is 1/3000 second and n is 5. Since the duty cycle used in this power converter is essentially for the bidirectional converter, meaning that the duty cycle, from 0~1, is able to control the flow of the current in two directions. Specifically, one direction of the current flow's duty cycle lies within the range of 0~0.5, and the opposite direction of the current flows in

the range of duty cycle 0.5~1. The direction of the power transmitted in one direction. And when the duty cycle lies in 0.5~1, it means the other direction. Meanwhile the DC energy acts as a power generator or motor depends on the supply-need characteristic. For the maximum power amount can be transmitted, we set the duty cycle to be 0.5. And we get the value of the inductor as putting every other component's value into the equation (49):

$$L_T = \frac{n \times V_H \times V_L \times T_s}{2P} \times d_h \times (1 - d_h). \tag{49}$$

We got the value of L_T is 5.208 *mH*. Now with the various amount of power transmission tasks, we use this calculated inductor value to configure the system and it is able to cover the maximum power transmitted through the cable. Then with the different value of amount of power transmitted, it needs to calculate the corresponding duty cycle for each power flow situation. And since there are two roots for the duty cycle as each of them indicates the direction of the transmitted power flow. For the study we analysis in this paper, the transmitted 100 kW power through the transmission system, then we will find the duty cycle's magnitude:

$$d_n - d_n^2 = \frac{2 \times P \times L_T}{n \times V_H \times V_L \times T}. \tag{50.1}$$

$$d_n = \frac{1 \pm \sqrt{1 - \frac{8 L_T P}{n \times V_H \times V_L \times T}}}{2}. \tag{50.2}$$

We will find that one solution of the duty cycle is to represent the power flows from the DC energy source to the power grid. As you can see in the whole calculation process, the central power unit is calculating the duty cycle online and then send the signal to local converter and give demand of certain value of the duty cycle. There is the inevitable time delay in the power transmission deployment because of the mechanism of the telecommunication and it has been shown that there are several time delays in the signal communication. It has also been shown that the time delay has an influence on the power system when the time delay is within the closed-

loop feedback. In this case, we've found that there is a significant impact on the system's output characteristic by having the time constant and therefore we need to find a way to solve the problem.

In the following sections, several methods to address this problem within the AC microgrid application shall be introduced.

4.4 SYSTEM MODEL DEVELOPMENT BY USING STATE SPACE EQUATION

In the previous paper, the controller is to address the instability caused by the negative incremental impedance in constant power load. The constant power load is the tightly regulated renewable generator with power converter. The controller's output is duty cycle and, by controlling of duty cycle, it is able to control the converter. The constant power load bears the nonlinearity characteristic and combined with the time delay, we need to linearize the system at certain operating point range where we can treat the overall system is linear. Previous literature and research have found a global solution to solve the negative incremental impedance in the system, however, such global control algorithm is not effective in addressing the time delay issue as well.

The system needs to be linearized at certain operating point and assume that the transmission system holds the dynamics at such operating point. The solution of controller is feasible when the system is running around the operating point. This method is feasible in reality as the power transmission system may have several different transmission tasks. Designer can calculate

several controller's parameters according to different transmission tasks. The duty cycle is an essential factor to control the power transmission system and unfortunately it has the time delay because of the telecommunication device characteristic. It is inevitable to somehow avoid the time delay in advance as the telecommunication system. The telecommunications system sends the duty cycle signal and causes the instability. The common way to represent the time delay in the frequency domain is using the exponential term.

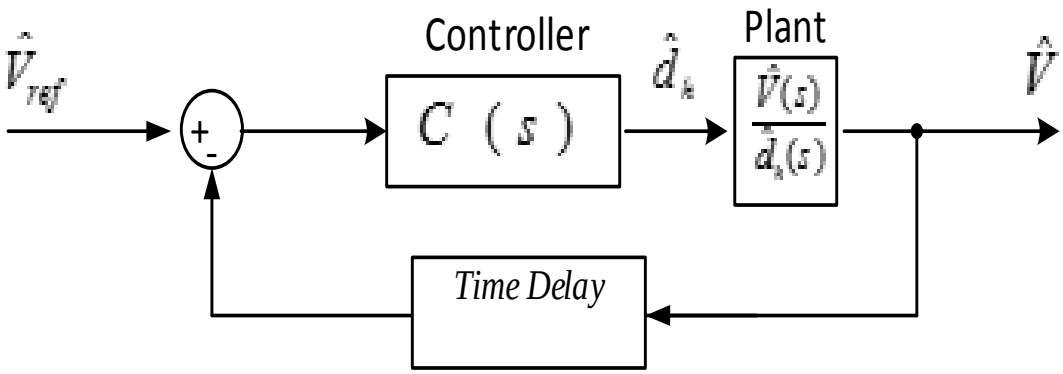

Figure 16: System dynamics in control block diagram form.

We'd like to introduce the state space equation for representing the entire system includes the power transmission system, constant power load and the time delay. The time delay's frequency domain representation is in exponential component term and it is very hard to analysis exponent term in the transfer function and therefore Padé approximation is introduced for building the entire system and developing controller. The Padé approximation represents the system with different order of transfer function and the generic representation is shown in the following. The higher order of the approximation, the more internal state variables are introduced and associated calculation needs to be conducted when defining the controller. The positive side is that we are able to achieve more accurate approximation and the controller will be more effective.

This is a generic form of the Padé approximation [57] in equation (51):

$$e^{-\tau s} \approx \frac{1 - k_1 s + k_2 s^2 + \cdots \pm k_n s^n}{1 + k_1 s + k_2 s^2 + \cdots \pm k_n s^n} \tag{51}$$

And as shown in the table below, it shows specific values of k_1, k_2,…, k_n and the values are related to the time delay. Simply put, if the approximation's order is 1, then the other k's value is zero and k_1 is $\tau/2$. And when the approximation's order is 2, then we will have two parameters: k_1 and k_2. It can be found that the reason why time delay causes the instability within the close-loop feedback control. One thing needs to notice is the tradeoff between the computation load versus the accuracy of the approximation. As seen in Figure 17, it is pretty brief approximation because there is only second order system. Surely we are able to represent the time delay with more accurate approximation, however, the undesired amount of computation and numerous internal number of states is another problem.

As we know that the key factor to determine the stability of system is by the poles' magnitude. As derived in equation (47), even with the system's stability, G(s), is assured, the overall close loop stability is shall be recalculated as the numerator of the time delay block is going to redefine the locations of the new poles and which can be positive poles and eventually causing the instability.

Table 3: Parameters for Pade Approximation.

Order	Numerical Quantity
n=1	$k_1 = \frac{\tau}{2}$, other $k_i = 0$
n=2	$k_1 = \frac{\tau}{2}, k_2 = \frac{\tau^2}{12}$, other $k_i = 0$

And therefore, the entire system can be studied as putting them in a cascade form. The transfer function of the dynamics of the duty cycle to the voltage output on the transmission receiver side can be represented as:

$$\frac{\hat{V}}{\hat{d}} = \frac{C(s)G(s)}{1 + e^{-\tau s}C(s)G(s)}$$

$$= \frac{C(s)G(s)}{1 + \frac{1 - \frac{\tau}{2}s}{1 + \frac{\tau}{2}}C(s)G(s)} \tag{52}$$

$$= \frac{\left(1 + \frac{\tau}{2}s\right)C(s)G(s)}{\left(1 + \frac{\tau}{2}s\right) + \left(1 - \frac{\tau}{s}s\right)C(s)G(s)}.$$

If the time delay, τ, is larger than one third of the time constant of the system, *G*(s), the term $1 - \frac{\tau}{2}s$, would cause positive poles in the transfer function and produce instability. And the negative effect caused by the time delay needs controller as well to addressing [58, 59].

As shown in the above derivation, the reason for the instability when the time delay is introduced is due to the positive zeros in the time delay approximation equation. As we assume that the given system in the denominator is stable, *C*(s)*G*(s), in other word, the poles of this system are negative poles. However, the additional terms related to the time delay may be potentially shifted in the poles from negative to positive. As long as the magnitude of the time delay exceeds one third of the time constant of the system, it will never be insignificant in the system.

With the high order of the system, it would be more straightforward to use state space equation and state feedback control to manipulate the poles of the integrated system: constant power load with the time delay. We need to integrate two systems in cascade to one system and develop controller from there.

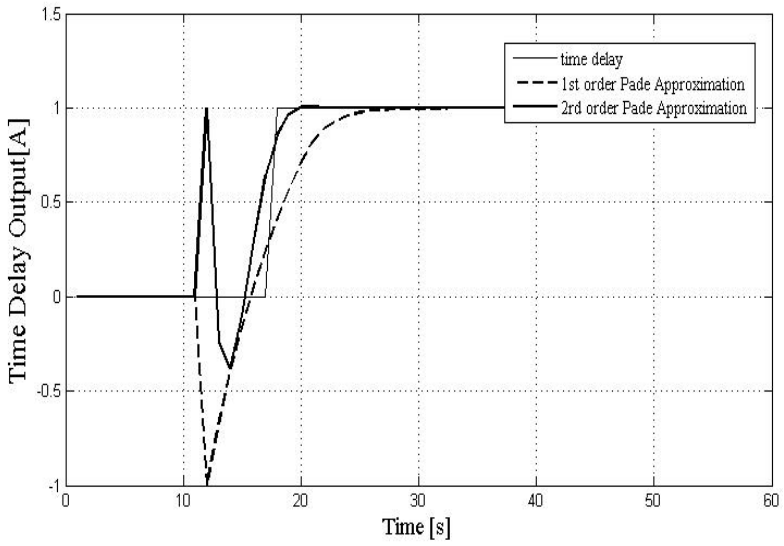

Figure 17: The approximation of time delay by using 1st and 2rd order system.

The duty cycle feeds into the power converter bears the following relationship and we transfer the time delay representation in exponential term into transfer function term, then eventually switches to state space equation representation for the controller development purpose.

$$\frac{\hat{d}_{delay}}{\hat{d}} = e^{-\tau s} \cong \frac{1-\tau s}{1+\tau s}$$

$$\begin{cases} dx = -\frac{1}{\tau}x + \hat{d} \\ \hat{d}_{delay} = \frac{1}{2\times\tau}x - \hat{d} \end{cases} \quad (53)$$

The approximation of the time delay is a first order system and, meanwhile, we introduce one additional state variable, x, in the state space equation. Recall the system configuration: the duty cycle goes into dc-dc converter and generates an equivalent current source. This current source goes through the transmission line and there is another dynamics in the transmission system.

There is an internal gain associated with the dynamics between the duty cycle to the current of the converter. And the current source is the input to the transmission system, which will be discussed later. Recall the dynamics between the duty cycle versus the change of the voltage output:

$$\frac{\hat{V}_{out}}{\hat{d}_h} = \frac{nV_{DC}T_s}{2L_T} d_h(1-2d_h) Z_{out} = \frac{nV_{DC}T_s}{2L_T} d_h(1-2d_h) \frac{\hat{V}_{out}}{\hat{I}_{AVG}} \quad (54.a)$$

$$\frac{\hat{I}_{AVG}}{\hat{d}_h} = \frac{nV_{DC}T_s}{2L_T} d_h(1-2d_h) \quad (54.a)$$

These manipulations provide the new dynamics between the changes of duty cycle versus the change of the converter current. And the input of the transmission system is the converter current. The following state space equations state the dynamics:

$$C_1 \frac{dV_{c1}}{dt} = I_{AVG} - i_L \quad (55.a)$$

$$L \frac{di_L}{dt} = V_{c1} - V_{c2} - i_L \times R \quad (55.b)$$

$$C_2 \frac{dV_{c2}}{dt} = I_L - i_R = I_L + \frac{V_{c2}}{Y}. \quad (55.c)$$

Y represents the resistor of the constant power load at certain operating point. The following figure shows the cascade configuration of the analyzed system with full state space feedback control. The controller's inputs are a measurement of current, and voltage in the system which are measurable. The output of the controller is the duty cycle which to the converter in physical meaning.

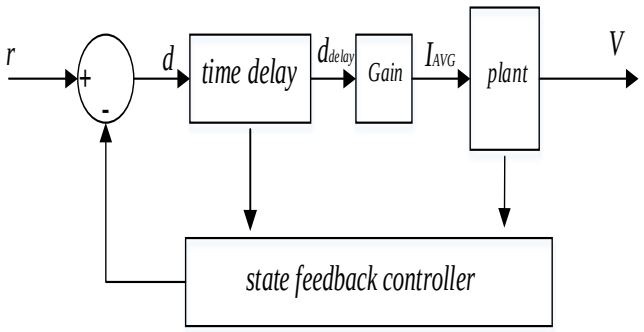

Figure 18: Configuration of the system with full-state feedback control.

There are four variables as state variables in the above equations, specifically: x= [V_{c1}, V_{c2}, i_L, x]^T. The integrated system's state space equation is shown in the following:

$$\begin{bmatrix} \dot{V}_1 \\ \dot{V}_2 \\ \dot{i}_L \\ \dot{x} \end{bmatrix} \approx \begin{bmatrix} 0 & 0 & -\frac{1}{C_1} & \frac{40}{C_1} \\ 0 & \frac{1}{YC_2} & \frac{1}{C_2} & 0 \\ \frac{1}{L} & -\frac{1}{L} & -\frac{R}{L} & 0 \\ 0 & 0 & 0 & -\frac{1}{\tau} \end{bmatrix} \begin{bmatrix} V_1 \\ V_2 \\ i_L \\ x \end{bmatrix} + \begin{bmatrix} -\frac{1}{C_1} \\ 0 \\ 0 \\ 0 \end{bmatrix} u \tag{56.a}$$

$$V_{out} = [1 \quad 0 \quad 0 \quad 0] \begin{bmatrix} V_1 \\ V_2 \\ i_L \\ x \end{bmatrix}. \tag{56.b}$$

The stability of the system is based on the matrix A in the state space equations (56) and matrix A is 4 by 4 in this case. The eigenvalues of matrix A is dependent on these parameters' values which are the electronic device components, internal values within the power converter and the duration of the time delay in practice. These values are shown in the Table 4[53]:

Table 4: Rated System Parameters [21].

Parameter	Numerical Quantity
Transformer Turns, n	5
Leakage Inductance, L_T	5.208 mH
Duty Cycle, d_h	0.1464
DC Bus Voltage, V_{DC}	1 kV
Switching Frequency, f_s	3 kHz
Line Resistance, R	0.0176 Ω/km
Line Inductance, L	0.248 mH/km
Line Capacitance, $2C_{1,2}$	0.923 μF/km
Lumped Capacitance, C_1	13.26 mF
Lumped Capacitance, C_2	5 mF
Cable Distance	0.1 km
Constant Power Load, Y	10 Ω_{DC}
Line Frequency	377 rad/s
Complex pole frequency, ω_1	3500 rad/s
Time Delay Duration, τ	0.2 sec

Based on Table 4, we are able to obtain zeros and poles of the system and plot them in the s-plane, as shown in the figure. And the data of this table is typical values of transmission line/cable's system parameters. And by using these parameters, we are able to analysis the stability of the power transmission system. From Figure 19, it is shown that there are two features of these poles distribution which lead to instability.

There are two aspects within this system by using the given parameters and therefore it causes problem: one is that there has one positive pole among four eigenvalues. And this positive pole contributes instability to the system. The other aspect of the system is because the other three poles having very undesirable values: small real part and significant large imaginary part. And their relative magnitude is quite different to each other. In term of system performance, the system has very large time constant/natural frequency, which is accorded to the reality. However it also has very small damping effect and thus whenever there has an oscillation, the system takes long time to recover. The result is the system has huge oscillation and it converges to the steady state very slowly.

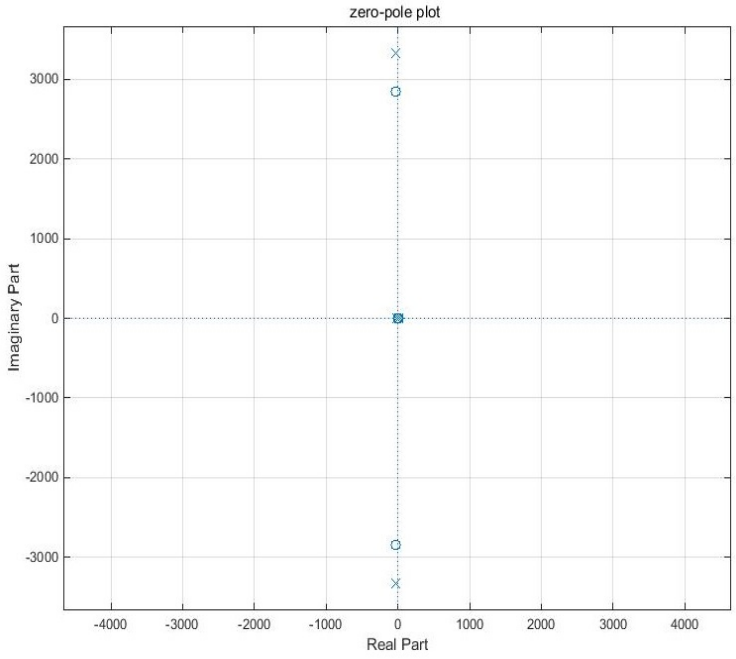

Figure 19: Plot of zeros and poles for the system.

Full state feedback control is to provide the gain control to change the poles in the overall system by introducing the vector *K*. Control vector, *K*, has the following form and it combine matrix *A* with vector *B* to generate a new matrix *A-BK*.

$$u = -Kx = -[k_1 \quad k_2 \quad k_3 \quad k_4]\begin{bmatrix} V_{c1} \\ V_{c2} \\ i_L \\ x \end{bmatrix}. \tag{57}$$

The new matrix of the state space equation is going to have poles designed by the user. The choice of the poles are suggested to be within the region shown in the Figure 21. It has relative large real part in the pole and small imaginary part. The underlying reason of such design philosophy is to build a system that has faster convergence rate with small oscillation.

And since the order of overall system is 4, then four poles are going to uniformly distributed on the arc of the shadow region as we'd like to have these four poles having almost the same contributing factors to the system. Also we don't want to tune the system with expensive

controller for the optimal performance as the absolute magnitude of these poles are quite large. And intuitively, the choice of the absolute poles' value should be reasonably to close to the original poles' absolute values with different locations in the s-plane.

Namely, these four poles are the new matrix and the task here is to find the vector *K* such that dynamics of the system changes. The choice of location of these poles is not unique as there is freedom according to the users' preference. If the user wants to achieve rigid transient performance with fast convergence and a small magnitude of the transient oscillation, the locations of these poles can be pure negative real values. If the user only wants to stabilize the system with a small budget, it is suggested to use the location of the poles in figure while the magnitude of these poles can be chosen larger.

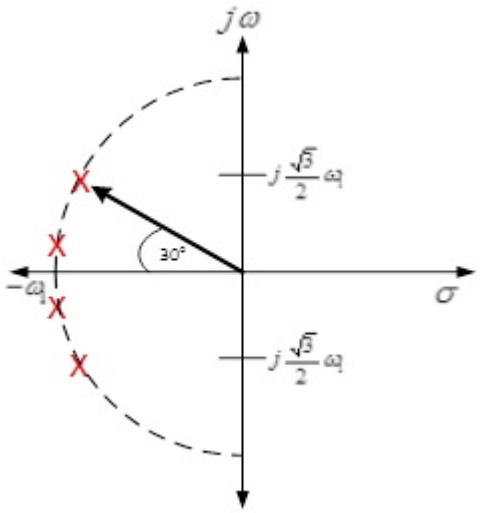

Figure 20: Poles location of the new system under the controller's effect.

Based on the discussion above, the magnitudes of poles mentioned above are intuitively picked as:

$$p_{1,2} = -43.3 \pm 25j \; and \; p_{1,2} = -49.24 \pm 8.7j. \tag{58}$$

And the vector K can be determined with these parameters:

$$K = [-2.0324 \quad 2.2969 \quad 3.6363 \quad -39.8601]. \tag{59}$$

The forth value in the controller vector *K* corresponds to the internal time delay state variable x. Different to the other three state variables which can be directly measured in the transmission system is that the forth state variable should be calculated. Recall the state space equation when the Pade approximation was introduced and then we are able to find the expression of this state variable:

$$x = 2\tau \times (d_{delay} + d). \tag{60}$$

There is only one state variable related to the time delay state. With higher approximation transfer function's order, there is going to have way more state variables introduced and more complicated mathematical expression should be calculated to find these state variables. We need to find the casual expression of such internal state and therefore they can actually be measured in practice

4.5 SYSTEM MODEL DEVELOPMENT USING MODEL MATCHING CONTROL

By finding the state feedback gain in the state space equation, we can see from the simulation result that the system goes to stable because of the time delay. It is worthwhile to mention that there is no way to fully eliminate the time delay in the system. Another common method, particularly used in addressing the time delay issue, is called the Smith Predictor Compensator. From the result, Figure 21, we can see that the system goes to stable although it

takes a while to converge to the steady state. Also there is a voltage sag within first around 0.6 second mark. This is because the positive zeros or non-minimal phase zeros' effect. Such issues can be further improved by introducing the model matching technique for designing the compensators. We do not want the system's response to have such characteristic and the reason is because of the positive zeros in the system. Therefore we will introduce the model matching for improvement.

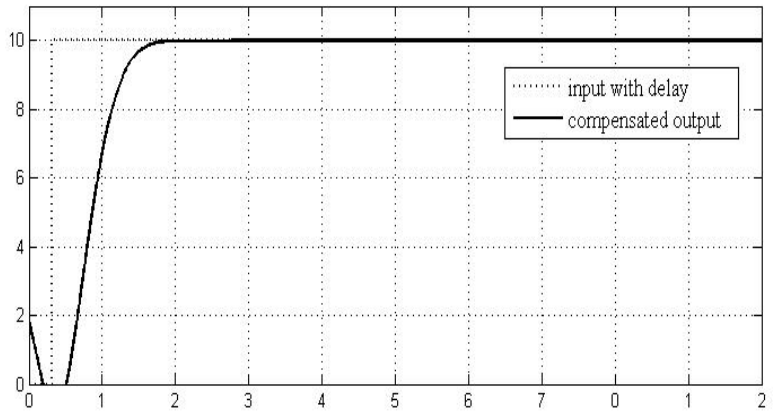

Figure 21: Dynamics of the CPL system using full state feedback controller.

Non-minimal phase zeros are contributed to the transient dynamics of the system. It doesn't cause any stability issues as only the location of poles are contributing to the system's stability. Using full state space feedback is only effective in improving the locations of poles while the model matching technique can improve the location of poles and minimal phase zeros. In other words, there is no effective way to solve the non-minimal phase zeros so far with the limitation associated with techniques. Nevertheless, we are able to break down the system into the part which is controllable and the other part which is non-controllable.

Model matching changes the poles and zeros in the transfer function according to the design procedure. Meanwhile, the non-minimal phase zeros (positive zeros) retain in the transfer

function. As a result, we are able to tune the tunable poles and zeros as much as we can to improve the given system.

As recall from previous results, the dynamics between the duty cycle to the converter to the output of the voltage on transmission receiver end bears the following relationship:

$$\frac{\hat{V}}{\hat{d}_h} = \frac{nV_{DC}T_s}{2L_T}(1-2d_h)Z_{out} \equiv K_{DC}Z_{out}. \tag{61.a}$$

$$Z_{out} = \frac{LC_2Ys^2 + (RC_2Y - L)s + (Y - R)}{LC_1C_2Ys^3 + (RC_1C_2Y - LC_1)s^2 + (C_1Y - RC_1 + C_2Y)s - 1}. \tag{61.b}$$

And then since the time delay of the duty cycle is in cascade to equation (61), it leads to the following overall system:

$$\frac{\hat{V}}{\hat{d}_{hdelay}} = \frac{\hat{V}}{\hat{d}_h}\frac{\hat{d}_h}{\hat{d}_{hdelay}} = \frac{nV_{DC}T_s}{2L_T}(1-2d_h)Z_{out}\frac{1-\frac{\tau}{2}s}{1+\frac{\tau}{2}s}. \tag{62}$$

Due to the controllable matrix calculated based on the analysis system is full rank, the system is entirely controllable. We need to check to make sure that the overall system is controllable. Otherwise, either the full state feedback controller or model matching controller will not be effectively working as control scheme is ineffective to those uncontrollable state variables. In equation (62) and thus we are able to obtain the poles and zeros. The transfer function is decomposed into the zero-pole form. Then we'd like to find the reference model, g_o(s), which is based on equation (58) and user design. We want g_o(s) to be close to the original system as much as possible for the cost of controller. And the transfer function derived from the system, g(s) and reference system g_o(s) should be implementable. The definition of implementable can be equivalent to the following points:

1). All the poles of g_o(s) should be negative;

2). The relative degree between the denominator and numerator in g_o(s) should be not less than that of g(s).

3). Non-minimal phase zeros in g(s) should be retained in g_o(s).

We need to find the compensators for the system with two freedom configuration. And the following is the procedure to find the compensators' parameters.

Firstly, let's define the given system's dynamics has the transfer function: g(s) =N(s)/D(s) and we assume they are coprime polynomial. And the reference model has dynamics: g_o(s) =E(s)/F(s). And therefore we compute equation (63) and cancel the common terms in the numerator and denominator. And we note the coprime terms as $\bar{E}(s)$ and $\bar{F}(s)$.

$$\frac{\hat{g}_o(s)}{N(s)} = \frac{E(s)}{F(s)N(s)} = \frac{\bar{E}(s)}{\bar{F}(s)}. \tag{63}$$

The equation represents that $\bar{E}(s)$ and $\bar{F}(s)$ are coprime. And now the reference model can be represented as in equation (64):

$$\hat{g}_o(s) = \frac{\bar{E}(s)N(s)}{\bar{F}(s)} = \frac{L(s)N(s)}{A(s)D(s) + M(s)N(s)}. \tag{64}$$

L(s), A(s) and M(s) are to be found and the proposed configuration of the control loop is shown in Figure 22 [60, 61]:

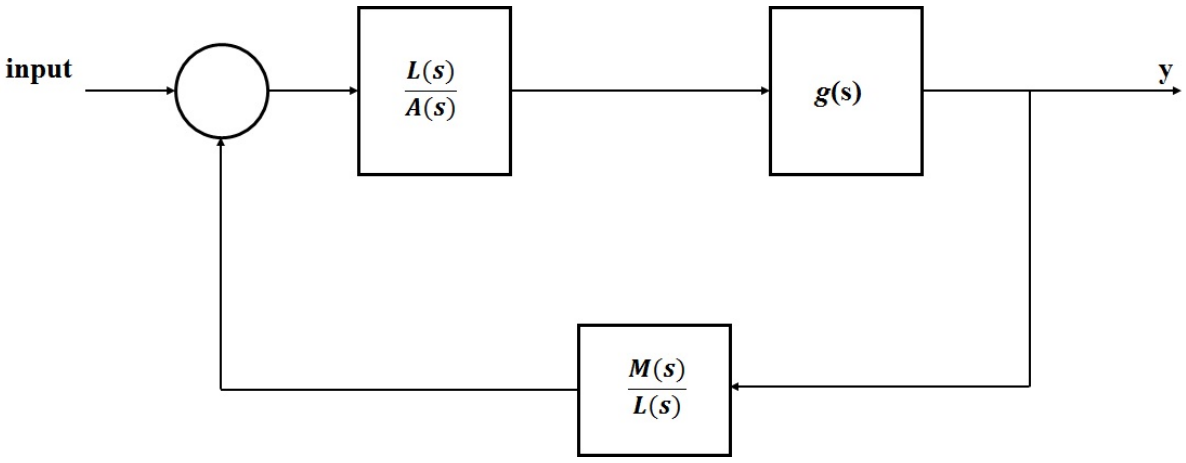

Figure 22: Topology of the controller for implementation of model matching algorithm.

In a simple put, the controller's structure is easy to implement and as shown in the figure, two block of the compensators: $\frac{L(s)}{A(s)}$ and $\frac{M(s)}{A(s)}$ are stable and therefore it is guaranteed that the system is implementable. To ensure that there is one solution for the linear equations, we need to make sure the denominator's order in in equation (65) should be at least 2n-1 where n is the degree of the denominator of the original system's order. The additional term to be adder is $\hat{F}(s)$ such that we multiple $\hat{F}(s)$ on the both side of system's transfer function and we are able to get the following equation:

$$\hat{g}_o(s) = \frac{\bar{E}(s)N(s)\hat{F}(s)}{\bar{F}(s)\hat{F}(s)} = \frac{L(s)N(s)}{A(s)D(s) + M(s)N(s)}. \tag{65}$$

We can find the unique solution of *A* and *M* matrix, respectively. And finally, we can find the polynomial term $L(s)$ as followed:

$$L(s) = \bar{E}(s)\hat{F}(s). \tag{66}$$

And to solve A(s) and M (s) in the denominator, we need to find the parameters:

$$A(s)D(s) + M(s)N(s) = \bar{F}(s)\hat{F}(s). \tag{67}$$

And to find the A(s), M(s), it is equivalent to solve the following linear equations:

$$\begin{aligned} A(s) &= A_0 + A_1 s + A_2 s^2 + \cdots + A_m s^m \\ M(s) &= M_0 + M_1 s + M_2 s^2 + \cdots + M_m s^m \\ \bar{F}(s)\hat{F}(s) &= F_0 + F_1 s + F_2 s^2 + \cdots + F_{n+m} s^{n+m}. \end{aligned} \tag{68}$$

Where $m \geq n-1$ and then the parameters of A(s) and M(s) are uniquely existed. To solve the equation (67), we could use equation (68):

$$[A_0 \quad M_0 \quad A_1 \quad M_1 \quad A_2 \quad \cdots \quad A_m \quad M_m] S_m = [F_0 \quad F_1 \quad \cdots \quad F_{n+m}]. \tag{69}$$

And therefore we are able to find the parameters of $A(s), M(s)$ and $L(s)$ and form the solutions. The configuration of the controller with the system is shown in the figure below. It is

more recommended to use the controller blocks in such form and thus the controllers are all proper in the application. Such arrangement can guarantee the overall system is stable. A brief description of the pros and cons by utilizing different topologies of these controller configuration will be put in the Appendix.

5.0 SIMULATION RESULTS AND DISCUSSION

5.1 MPPT AND RCC DECOUPLING RESULTS

The work to prove the validation of these methods is done in Simulink as simulation. In the appendix, it demonstrates the configuration of the simulation. It is proven theoretically that the MRAC and RCC are asymptotically converging to zero error. However, it is very critical that by decoupling these two algorithms together, the entire proposed hierarchal control is stable by analytical proving. As we mentioned above, the time constant of these two algorithms determines whether they can work together or not. RCC algorithm is to track the solar irradiance's effect on the duty cycle feed to the power converter. And therefore by choosing the significant difference between two control schemes time constant will result these two controls work independently to each other. As we may intuitively conclude that the time constant for RCC will be larger than the time constant of the MRAC. And it should be noted that the RCC's time constant also depends on the location of the initial guess. While the time constant of MRAC is tunable by assigning gain matrix in the equation.

Firstly, I showed the simulation result of the converter's voltage output. The voltage output is due to the change of the duty cycle and essentially is the result of the solar irradiance [27, 62].

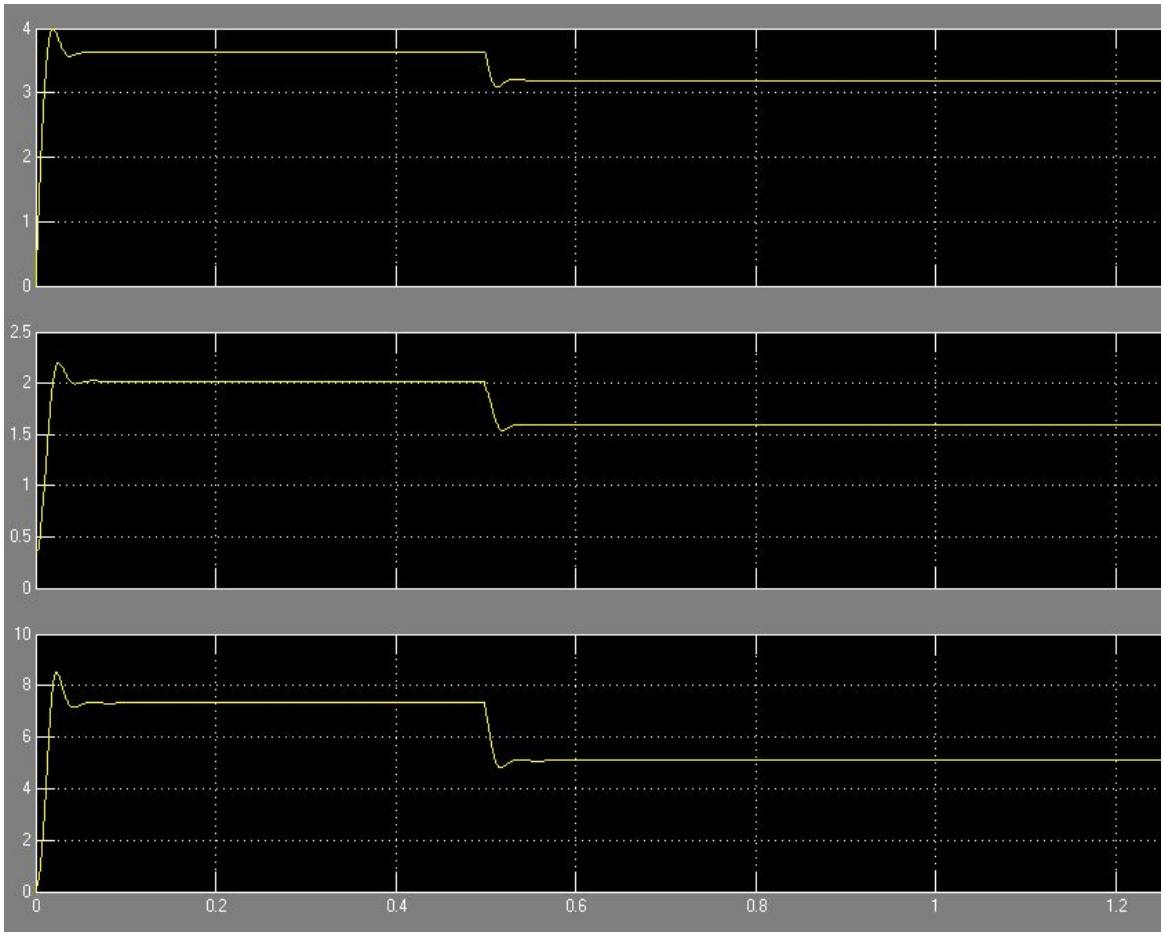

Figure 23: PV model's voltage output's transient response to duty cycle change.

And by having the oscillation and if we zoom the transient phase of the voltage change, it has the under damping characteristic. This is the key part in the voltage and need to use MRAC to tune such behavior. In the following table, it shows the basic configuration's parameters to run the simulation. And also since the adaptive control is implemented on the dynamic system of the solar conversion system, the reference model should be developed by the user and generate the adaptive control actions based on that.

Table 5: Boost Converter Parameters.

Circuit Parameters	Value
R_I	45 Ω
L_O	600 μ H
C_I	100 μ F
V_O	350 V

Table 6: Parameters in Adaptive Controller.

Circuit Parameters	Value
$k_p = {V_O}/{(L_O C_I)}$	$5.83*10^9$ V(rad/sec)^2
$a_p = 1/(R_I C_I)$	222 rad/sec
$b_p = 1/(L_O C_I)$	1.67×10^7 (rad/sec)^2
k_m	5.831×10^9 (rad/sec)^2
a_m	8.17×10^3 (rad/sec)
b_m	1.67×10^3 (rad/sec)^2
λ	1
g	1
Γ	5 × identity matrix

These parameters are used in the simulation of the MRAC and these data are originated from [18]. According to these parameters, the calculated damping ratio is less than 1, in other word, it will show the oscillation in the transient phase and such oscillation results as energy usage waste. These are because the external environment perturbance and it causes the system to operate at a new operating point. The reference model was designed to deliver a theoretical

maximum power point voltage by carrying a critically damped step response. The damping ratio, as shown in (6), its mathematical expression is $\frac{a_m}{2\sqrt{b_m}}$ and the designed reference system's damping ratio is chosen to be either exactly or slight less than 1. By choosing the damping ratio to be less than 1 is under the consideration for the system to response a little faster and may cause very little a bit of overshoot in the step response. The desired outcome of simulation would be that after the plant has undergone the adaptation phase, the parameters of the controlled plant would converge to the parameters of the reference model and therefore the adapted array voltage would show critically damped behavior.

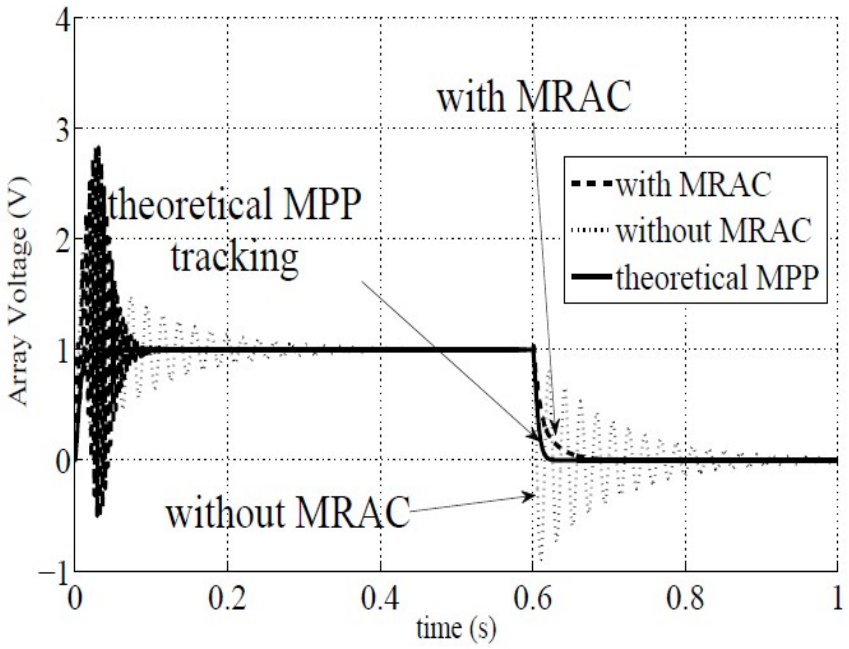

Figure 24: Initial stage of system's voltage step responses.

In Figure 22, it shows the characteristic of the plant model's change along the time. The step response is be altered into the pulse width modulation signal and each pulse, which is

having the exact same characteristic as one step function. Along each pulse stage or each step response, the process of adaptation can be well observed.

The system is the characteristic response when the input is the duty cycle change from the RCC and the output is the solar panel's voltage change. The figure shows three sets of step responses aligned together to deliver a clear comparison, which is the initial stage of the system. Three sets of system are undergoing the test: one is the system without using MRAC; one is the system using the MRAC and the other one is the step response of the reference model. From the figure, it shows that the system without using MRAC has an undesired transient oscillation. The system using the MRAC, swiftly converges to the reference model by taking two periods. As seen in the control law in previous paragraph, the converging rate of the system during the adaption process is depending on the Γ matrix, which is a diagonal matrix having a pure gain. The larger the gain is, the faster convergence rate it has. The initial stage where the system changes under the effect of controller last for 20 milliseconds and at 12 milliseconds, the solar insolation changes and the un-adapted voltage shows an underdamped response. Although the system using the MRAC exhibits slightly different in the voltage output, it shows much better result comparing to the system without using the MRAC. And therefore at 0.2 second around, which the system response is shown in the lower figure that the characteristic of the system with MRAC is almost the same characteristic of the reference system. And the step function fed to the system as an input is analog to the abrupt change in the duty cycle. And such change in the duty cycle is the worst case to consider. Confidently, the system's learning curve by using the MRAC controller with the worst input still shows the promising result.

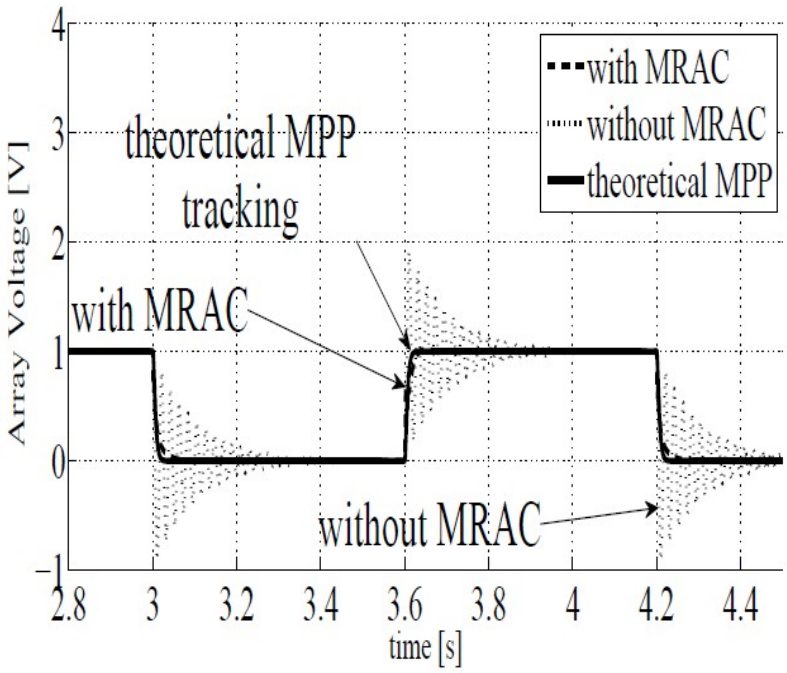

Figure 25: Later stage of system's step response after adaptation.

Figure 25 shows the system's performance at late stage. As seen from the figure, the system without using MRAC still carries under damping oscillation at each step change of the duty cycle. The time in Figure 26 is much larger than the time which the system takes to learn from the reference model and when time reaches 2 second, the system, under the effect of the controller, already bears the characteristic of the reference model plant. To approach to the maximum power point, corresponding voltage change are made to compensate the voltage to approach to the nominal voltage level. And the observation of the convergence for the plant model system can be found also in the error signal profile. In the error signal, it gives a straightforward comparison between the reference system's response to the non-using MRAC plant model and the reference system's response to the using MRAC plant model's response. As seen in the Figure 26, the error signal between the reference system's response and the plant

model's response is almost zero all along, except small-duration spike at each step occurring, which is inevitable and negligible.

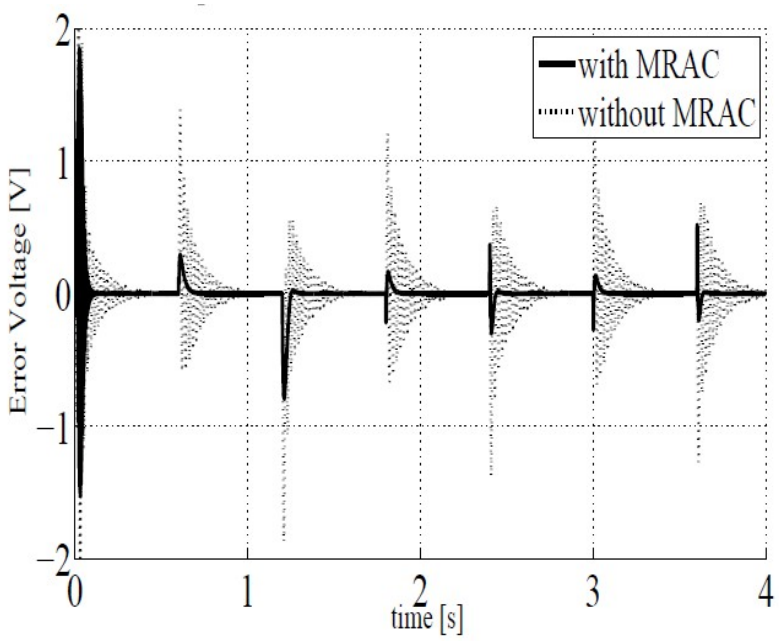

Figure 26: The error signals of the system compared to the reference model's response.

Theoretically, to guarantee the robust performance of the controller under the effect of noise and other signals' influence, the controller's parameters are calculated to demonstrate that whether the convergence of the system is genuine convergence, in other words, whether the difference of the controller's parameters approaches to zero. During the simulation, the values of the controller's parameters are approaching to the nominal parameters, which are the ones by equating the reference system model with the plant system and the controller's effect:

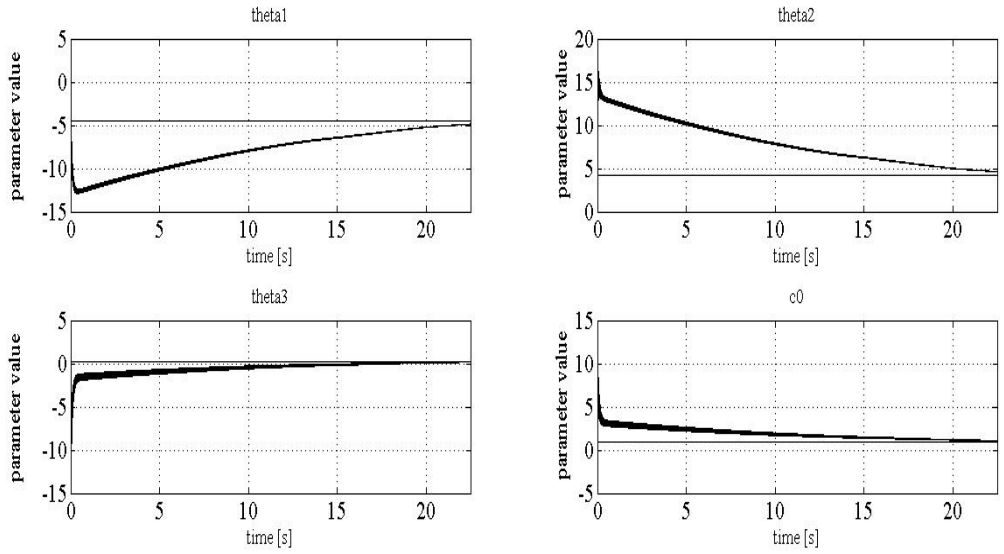

Figure 27: the controller parameter's converging curves.

Table 7: Comparison between Nominal and Actual Controller Parameters.

Circuit Parameters	θ_0	θ_1	θ_2	θ_3
Nominal controller parameters	1	-7.95×10^{3}	-22.8	-3.00×10^{-4}
Updated controller parameters	1	-8.12×10^{3}	-20.4	-2.8×10^{-4}

Based on the Table 7, it shows that the controller parameters, after around 0.2 second's update from the adaptive controller, and the parameters' difference is negligible. And therefore, this table's data is sufficient enough to conclude that this adaptive controller adapted the characteristic of the plant model.

Next subsection is to show the result obtained in the RCC algorithm. The goal of showing result of RCC is to show the validation of the RCC and its realization in the simulation.

1) Ripple Correlation Control

Ripple Correlation Control is utilizing the ripple component of the voltage and the current from the solar panel to calculate where is the reference location to the maximum power point (MPP). The control law of ripple correlation control has been discussed in the previous section. In this section, it briefly presents the simulation results obtained in the Simulink of utilizing RCC in the solar panel. Due to the complexity of the real time simulator in the project, we are only to use the emulator to mimic the effect of the solar irradiance and therefore the results shown below don't exhibit too much difference. However, especially under extreme situation where the solar irradiance changes dramatically, the filter is going to filter out the high frequency components and meanwhile maintain the control algorithms are able to decouple.

From Figure 25, the boost converter is used to increase or decrease the voltage value of the solar panel, in term to change the operating point of the solar panel and make sure the solar panel is working around close enough to the MPP. And therefore, on the solar panel side of the small signal circuit, the small signal circuit which is used to study the dynamic performance of the entire system can be viewed as follows:

In the simulation conducted in the Simulink, the following figures illustrates the transient dynamics when the solar irradiance changes and therefore the voltage decrease to a new level and therefore the oscillation could be observed.

5.2 MICROGRID POWER TRANSMISSION SYSTEM RESULTS

The result is shown in the Figure 28, and it shows the voltage output of bidirectional DC/DC converter. Firstly, it is very important to note that by using Full State Feedback Control (FSFC) and the Model Matching Control (MMC), the voltage output through the transmission system and included with the time delay becomes stable. Such results demonstrate that these two methods used in this paper are both effective. Secondly, by introducing new zeros because of either the existence of relative large inductor in the transmission system or the existence of large time feedback delay in the centralized control, model matching control is able to improve the transient characteristic of the voltage output to certain extend. As it shows clearly that the voltage

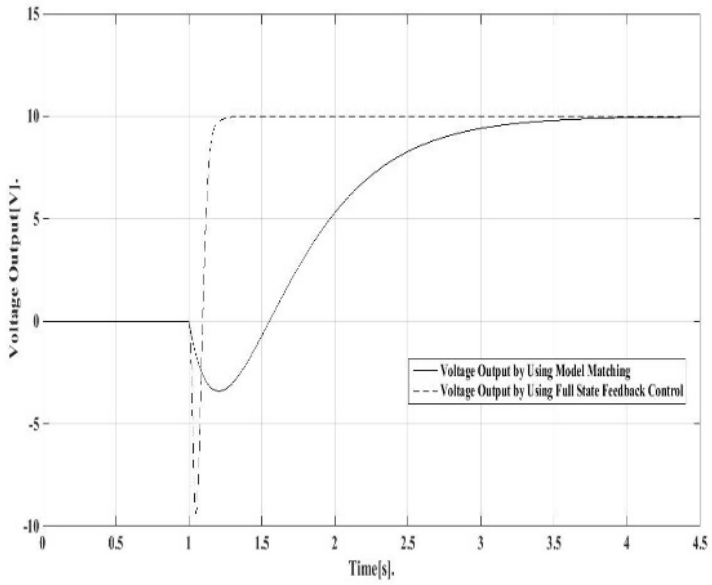

Figure 28: Comparison of the Voltage Output Response by using two methods.

drop at the step response has been significantly decreased. And also the time taken to approach to the steady state has been increased. Such behavior is more recommended as in the power system, the entire system's response is quite slow and therefore it avoid unnecessary energy wasted in the controller and the control is smoother.

In summary, this paper introduces one method to addressing the instability issue caused by constant power load's negative incremental impedance and another two methods in addressing the instability issue caused by the constant power load and the telecommunication time delay. Each method has certain connection with each other and indeed based upon the simulation result, the voltage output has been improved significantly. And also just as shown the comparison of voltage outputs by using different methods, it provide advantages and disadvantage of using these different controllers, according to users' choice.

One more thing needs to notice is that in each scenario, we consider the time delay is 0.2 second as it is the maximum time delay in practice. Same as the operating point of the constant power load, in another word, we had a strong assumption that the overall system is working in certain condition and will not change the operating point too often in operation. And the following methods are all in domain of linear system analysis and locally effective. In the next paper, we are going to present the global controller development by introducing the adaptive control as we only give the overall system with desired performance and the controller will adaptively tune the system and control the system's output. The advantage of using adaptive control will eliminate the numerous offline calculation if the system is operating in different operation points. Instead, it is going to do the online calculation and control the system.

6.0 CONCLUSION

The results in Chapter 5 shows the effectiveness of using adaptive control in improving the energy conversion efficiency in the MPPT and therefore the voltage output shows smoother convergence curve in the transient dynamics of the system. The MPPT algorithm's realization is based on the foundation that two control schemes can be decoupled together. And the full state feedback control and model matching control techniques are trying to mitigate the effect by redistribute the locations of the poles and minimal phase zeros in the system and therefore the stability of the system can be assured. Moreover, better transient response can be improved.

As we are pacing with the progress of technology revolution where we will expect more and more distributed variable renewable generators or energy sources in the field. Many realistic issues cannot be encountered through the analysis and they are more likely to encounter through the experiment or real life. We may not expect the time delay issue by just doing the simulation as there are always some assumptions that require us to simplify the problem or which are even beyond our consideration.

This work comprehensively illustrates the essential contribution by developing control techniques by using modern control design techniques. These methods are more versatile and effective to deal with the situations in practice[63].

As we may discuss within the previous sections, there are going to have many more work need to be done and uncover the field where have lots of fruit. For example, how to simplify the

control implementation as adaptive control is rather complicate to realize and the computation work, depending on the size of the system, should be completed as more advanced computing unit, such as computer. We need to come up more simplified control realization and therefore we can implement these advanced control schemes on the board.

Moreover, as we have tasted the flavor of the adaptive control in addressing different types of problems and how robust it is when we are no longer to require the wholesome information of the system. We could develop the model reference adaptive control to address the constant power load stability issue in sense of global. The work is not trivial and requires more effort to come up the solution. And also as having been emphasized several times that the critical meaning of CPL, the developing of such method is definitely required.

APPENDIX

THE PRELIMINARIES AND RELATED CODES

Solar Panel’s simulation model code

The following code exhibits the way to model the solar panel in the work:

```
function SimpleSolarCellAndPanelModel

   %Define Voltage
   Va = 0:0.01:1.665;

   subplot(2,1,1);
   title('Sunpower cell current/voltage')
   hold on
   plot(dataU, dataI, 'r', 'LineWidth', 1);
   plot(Va, solar(Va,1,25), 'b-', 'LineWidth', 1)
   plot(Va, solar(Va,1,40), 'b--', 'LineWidth', 1)
   plot(Va, solar(Va,1,55), 'b-.', 'LineWidth', 1)
   plot(Va, solar(Va,1,70), 'b:', 'LineWidth', 1)
   ylim([0,Inf]);
```

```
xlabel('Voltage [V]');
ylabel('Current [A]');
grid on

subplot(2,1,2);

hold on
plot(dataU, dataU.*dataI, 'r', 'LineWidth', 1);
plot(Va, Va.*solar(Va,1,25), 'b-', 'LineWidth', 1)
plot(Va, Va.*solar(Va,0.75,40), 'b--', 'LineWidth', 1)
plot(Va, Va.*solar(Va,0.5,55), 'b-.', 'LineWidth', 1)
plot(Va, Va.*solar(Va,0.25,70), 'b:', 'LineWidth', 1)
ylim([0,Inf]);
xlabel('Voltage [V]');
ylabel('Power [W]');
grid on
```

Model Matching and Full State Space Feedback simuation code:

```
clc;
clear all;

d= 0.1;
```

```
n=5;

Vdc=1000;

Ts=1/3000;

Lt=5.208e-3;


% DC Resistance at 20 degrees

R_m = 0.0176;                %ohm/km

R = R_m*d;                   %ohm


% Trefoil Formation

L_m = 0.248e-3;              %H/km

L = 10*L_m*d;                %H


% Nominal Capacity

C_m = 0.923e-6;              %F/km

C = C_m/2*d;


C1 = 13.2e-3;

C2 = 5e-3;

Y=25;

%Y2=50;

%Y3=75;

Kdc=(n*Vdc*Ts*(1-2*0.14))/(2*Lt);
```

```
s=tf('s');
x2 = Y*C2*L;
x1 = R*C2*Y-L;
x0 = Y-R;
y3 = L*C1*C2*Y;
y2 = R*C1*C2*Y-L*C1;
y1 = C1*Y-R*C1 + C2*Y;
y0 = -1;
sys = Kdc * tf([x2 x1 x0],[y3 y2 y1 y0]); % three order system
zplane([x2 x1 x0],[y3 y2 y1 y0]);

D=[-1 0.455 -3.696e-7 4.092e-07 0 0];
N=[2880 -0.003226 0.003571 0 0 0];
D1=[0 -1 0.455 -3.696e-7 4.092e-07 0];
N1=[0 2880 -0.003226 0.003571 0 0];
D2=[0 0 -1 0.455 -3.696e-7 4.092e-07];
N2=[0 0 2880 -0.003226 0.003571 0];
Sm=[D;N;D1;N1;D2;N2]';

L=-1.753e10 - 1.685e7*s - 4012*s^2;%order from low to high order coefficients
F=[4.286e16 1.012e14 9.556e10 4.507e7 10618 1]';
%AM=Sm\F;
```

```
AM=bicgstab(Sm,F,[],20);
AM=AM';
AA1=AM(1,1);
AA2=AM(1,3);
AA3=AM(1,5);
MM1=AM(1,2);
MM2=AM(1,4);
MM3=AM(1,6);
AA = 37.9401*s^2 + 3.6981e8*s + 2.2244e11;
MM = 1.4959e10 + 1.3419e7 * s + 7.6608e-4 * s^2;
N=0.003571*s^2 - 0.003226*s + 2880;
D=4.092e-07*s^3 - 3.696e-07*s^2 + 0.455*s - 1;
sys_test=(L*N)/(AA*D+MM*N);
%============================================================
%for the nonminimal phase zeros

% L=-[158.3 5.917 0.0553];%order from low to high order coefficients
% F=[2.558e8 3.656e7 1.763e6 37442 345 1]';
% %AM=Sm\F;
% AM=bicgstab(Sm,F,[],20);
% AM=AM';
% AA = 37.9401*s^2 + 3.6981e8*s + 2.2244e14;
% MM = 1.4959e13+1.3419e7 * s + 7.6608e-4 * s^2;
```

```
%============================================================
%sys_new1=-(4012* s^2+1685e7 *s +1.753e10 )* (0.003571 *s^2 -0.003226 * s +2880);
%sys_new2=(1.4959e13+1.3419e7 * s + 7.6608e-4 * s^2)*(0.003571 *s^2-
0.003226*s+2880)+(37.9401 * s^2+3.6981e8 *s +2.2244e14)*(4.092e-07* s^3 - 3.696e-07* s^2
+ 0.455* s - 1);
%sys_new=(sys_new1)/(sys_new2);
%new_sys=LN/(MN+AD)

%num=[-5.714e-05 -0.002341 -460.7 4607];
%den=[6.547e-09 3.992e-07 0.07279 0.3279 -4]; %num and den are obtained from
sys_delay
%num1=[0.0001429 0.007281 1152];
%den1=[1.637e-08 8.342e-07 0.182 -1]; %num and den are obtained from sys
%D=[-1000 455 0.002577 4.092e-05 0 0];
%N=[2880 0.02249 0.0003571 0 0 0];
%D1=[0 -1000 455 0.002577 4.092e-05 0];
%N1=[0 2880 0.02249 0.0003571 0 0];
%D2=[0 0 -1000 455 0.002577 4.092e-05];
%N2=[0 0 2880 0.02249 0.0003571 0];
%Sm=[D;N;D1;N1;D2;N2]';
%i pick poles are -3500,-3300+/-40i
%i pick zeros are -2830+/-20i
```

```
%================================================
%ref system two
%L=-[9.64e10 6.783e7 11946];%order from low to high order coefficients
%F=[2.356e18 2.212e15 9.898e11 3.477e8 8.494e4 8.728]';
%AM=Sm\F;
%AM=AM';
%AA = -4.2427e-16 - 3.9842e-19 * s - 1.7829e-22 * s^2;
%MM = 1.2224e-15 + 1.1477e-18 * s + 5.1356e-22 * s^2;
%================================================
%ref system one
%L=-[6434 398.6 6.228];%order from low to high order coefficients
%F=[1.572e11 1.734e10 6.453e08 8.071e6 143 1]';
%AM=F\Sm;
%AM=AM';
%AA=-5.9693e-9-(6.815e-10)*s-s^2*2.5652e-11;
%MM=1.81e-8+1.9965e-9*s+7.43e-11*s^2;
%================================================
%%%different solver
%AM=bicgstab(Sm,F,[],20);
%AM=AM';
%================================================
```

BIBLIOGRAPHY

[1] S. Lindenberg, *20% Wind Energy By 2030: Increasing Wind Energy¿ s Contribution to US Electricity Supply*: DIANE Publishing, 2009.

[2] Y. Liang, Z. Xu, J. Xia, S. T. Tsai, Y. Wu, G. Li, *et al.*, "For the bright future bulk heterojunction polymer solar cells with power conversion efficiency of 7.4%," *Advanced Materials,* vol. 22, 2010.

[3] H. K. Khalil and J. Grizzle, *Nonlinear systems* vol. 3: Prentice hall New Jersey, 1996.

[4] M. Krstic, P. V. Kokotovic, and I. Kanellakopoulos, *Nonlinear and adaptive control design*: John Wiley & Sons, Inc., 1995.

[5] D. P. Bertsekas, D. P. Bertsekas, D. P. Bertsekas, and D. P. Bertsekas, *Dynamic programming and optimal control* vol. 1: Athena Scientific Belmont, MA, 1995.

[6] H. Kwakernaak and R. Sivan, *Linear optimal control systems* vol. 1: Wiley-interscience New York, 1972.

[7] F. Blaabjerg, R. Teodorescu, M. Liserre, and A. V. Timbus, "Overview of control and grid synchronization for distributed power generation systems," *Industrial Electronics, IEEE Transactions on,* vol. 53, pp. 1398-1409, 2006.

[8] P. Rao, M. Crow, and Z. Yang, "STATCOM control for power system voltage control applications," *Power Delivery, IEEE Transactions on,* vol. 15, pp. 1311-1317, 2000.

[9] M. Yamamoto and O. Motoyoshi, "Active and reactive power control for doubly-fed wound rotor induction generator," *Power Electronics, IEEE Transactions on,* vol. 6, pp. 624-629, 1991.

[10] W. E. Dixon, A. Behal, D. M. Dawson, and S. P. Nagarkatti, *Nonlinear control of engineering systems: a Lyapunov-based approach*: Springer Science & Business Media, 2013.

[11] R. Freeman and P. V. Kokotovic, *Robust nonlinear control design: state-space and Lyapunov techniques*: Springer Science & Business Media, 2008.

[12] A. K. Abdelsalam, A. M. Massoud, S. Ahmed, and P. N. Enjeti, "High-performance adaptive perturb and observe MPPT technique for photovoltaic-based microgrids," *Power Electronics, IEEE Transactions on,* vol. 26, pp. 1010-1021, 2011.

[13] N. Femia, G. Petrone, G. Spagnuolo, and M. Vitelli, "Optimization of perturb and observe maximum power point tracking method," *Power Electronics, IEEE Transactions on,* vol. 20, pp. 963-973, 2005.

[14] D. Sera, L. Mathe, T. Kerekes, S. V. Spataru, and R. Teodorescu, "On the perturb-and-observe and incremental conductance MPPT methods for PV systems," *Photovoltaics, IEEE Journal of,* vol. 3, pp. 1070-1078, 2013.

[15] G. J. Kish, J. J. Lee, and P. Lehn, "Modelling and control of photovoltaic panels utilising the incremental conductance method for maximum power point tracking," *Renewable Power Generation, IET,* vol. 6, pp. 259-266, 2012.

[16] D. Sera, L. Mathe, and F. Blaabjerg, "Distributed control of PV strings with module integrated converters in presence of a central MPPT," in *Energy Conversion Congress and Exposition (ECCE), 2014 IEEE,* 2014, pp. 1-8.

[17] P. Sharma and V. Agarwal, "Exact Maximum Power Point Tracking of Grid Connected Partially Shaded PV Source Using Current Compensation Concept," 2013.

[18] M. Veerachary, T. Senjyu, and K. Uezato, "Neural-network-based maximum-power-point tracking of coupled-inductor interleaved-boost-converter-supplied PV system using fuzzy controller," *Industrial Electronics, IEEE Transactions on,* vol. 50, pp. 749-758, 2003.

[19] C.-S. Chiu, "TS fuzzy maximum power point tracking control of solar power generation systems," *Energy Conversion, IEEE Transactions on,* vol. 25, pp. 1123-1132, 2010.

[20] H. Heydari-doostabad, R. Keypour, M. R. Khalghani, and M. H. Khooban, "A new approach in MPPT for photovoltaic array based on extremum seeking control under uniform and non-uniform irradiances," *Solar Energy,* vol. 94, pp. 28-36, 2013.

[21] E. V. Solodovnik, S. Liu, and R. A. Dougal, "Power controller design for maximum power tracking in solar installations," *Power Electronics, IEEE Transactions on,* vol. 19, pp. 1295-1304, 2004.

[22] S. L. Brunton, C. W. Rowley, S. R. Kulkarni, and C. Clarkson, "Maximum power point tracking for photovoltaic optimization using ripple-based extremum seeking control," *Power Electronics, IEEE Transactions on,* vol. 25, pp. 2531-2540, 2010.

[23] T. Esram and P. L. Chapman, "Comparison of photovoltaic array maximum power point tracking techniques," *Energy conversion, IEEE transactions on,* vol. 22, pp. 439-449, 2007.

[24] T. Esram, J. W. Kimball, P. T. Krein, P. L. Chapman, and P. Midya, "Dynamic maximum power point tracking of photovoltaic arrays using ripple correlation control," *Power Electronics, IEEE Transactions on,* vol. 21, pp. 1282-1291, 2006.

[25] G. Irisarri, X. Wang, J. Tong, and S. Mokhtari, "Maximum loadability of power systems using interior point nonlinear optimization method," *Power Systems, IEEE Transactions on,* vol. 12, pp. 162-172, 1997.

[26] S. Jain and V. Agarwal, "A new algorithm for rapid tracking of approximate maximum power point in photovoltaic systems," *Power Electronics Letters, IEEE,* vol. 2, pp. 16-19, 2004.

[27] R. Khanna, Q. Zhang, W. Stanchina, G. Reed, and Z. Mao, "Maximum power point tracking using model reference adaptive control," 2014.

[28] J. W. Kimball and P. T. Krein, "Discrete-time ripple correlation control for maximum power point tracking," *Power Electronics, IEEE Transactions on,* vol. 23, pp. 2353-2362, 2008.

[29] D. Marx, P. Magne, B. Nahid-Mobarakeh, S. Pierfederici, and B. Davat, "Large signal stability analysis tools in DC power systems with constant power loads and variable power loadsâ€”A review," *Power Electronics, IEEE Transactions on,* vol. 27, pp. 1773-1787, 2012.

[30] A. Agarwal, K. Deekshitha, S. Singh, and D. Fulwani, "Sliding mode control of a bidirectional DC/DC converter with constant power load," in *DC Microgrids (ICDCM), 2015 IEEE First International Conference on*, 2015, pp. 287-292.

[31] W. Du, J. Zhang, Y. Zhang, and Z. Qian, "Stability criterion for cascaded system with constant power load," *Power Electronics, IEEE Transactions on,* vol. 28, pp. 1843-1851, 2013.

[32] P. Magne, D. Marx, B. Nahid-Mobarakeh, and S. Pierfederici, "Large-signal stabilization of a dc-link supplying a constant power load using a virtual capacitor: impact on the domain of attraction," *Industry Applications, IEEE Transactions on,* vol. 48, pp. 878-887, 2012.

[33] K. J. Ãstrom and B. r. Wittenmark, *Adaptive control*: Courier Corporation, 2013.

[34] C. Frohlich, "Total solar irradiance observations," *Surveys in geophysics,* vol. 33, pp. 453-473, 2012.

[35] P. Suskis and I. Galkin, "Enhanced photovoltaic panel model for MATLAB-simulink environment considering solar cell junction capacitance," in *Industrial Electronics Society, IECON 2013-39th Annual Conference of the IEEE*, 2013, pp. 1613-1618.

[36] J.-H. Jung and S. Ahmed, "Real-time simulation model development of single crystalline photovoltaic panels using fast computation methods," *Solar Energy*, vol. 86, pp. 1826-1837, 2012.

[37] P. Pourmohammadi, S. P. Chalsaraei, R. Khodadadi, M. A. Ghasemi, and H. Ghorbanpour, "Third order butterworth bandpass filter using active inductor," *International Journal of Engineering Research and Applications*, vol. 2, p. 2754, 2012.

[38] A. Sapin, P. K. Steimer, and J.-J. Simond, "Modeling, simulation, and test of a three-level voltage-source inverter with output LC filter and direct torque control," *Industry Applications, IEEE Transactions on*, vol. 43, pp. 469-475, 2007.

[39] C. Madsen, "Efficient architectures for exactly realizing optical filters with optimum bandpass designs," *Photonics Technology Letters, IEEE*, vol. 10, pp. 1136-1138, 1998.

[40] S. Sastry and M. Bodson, *Adaptive control: stability, convergence and robustness*: Dover Publications, 2011.

[41] I. D. Landau, R. Lozano, M. M'Saad, and A. Karimi, *Adaptive control* vol. 51: Springer Berlin, 1998.

[42] K. Narendra and L. Valavani, "Stable adaptive controller design--Direct control," *Automatic Control, IEEE Transactions on*, vol. 23, pp. 570-583, 1978.

[43] C. Hollot, L. Huang, and Z.-L. Xu, "Designing strictly positive real transfer function families: A necessary and sufficient condition for low degree and structured families," *Proc. of Mathematical Theory of Network and Systems*, pp. 215-227, 1990.

[44] W. Sun, P. P. Khargonekar, and D. Shim, "Solution to the positive real control problem for linear time-invariant systems," *Automatic Control, IEEE Transactions on*, vol. 39, pp. 2034-2046, 1994.

[45] H. Ho Choi and M. Jin Chung, "Estimation of the asymptotic stability region of uncertain systems with bounded sliding mode controllers," *Automatic Control, IEEE Transactions on*, vol. 39, pp. 2275-2278, 1994.

[46] E. Baring-Gould, "Village microgrids: The Chile project," National Renewable Energy Lab., Golden, CO (United States)1997.

[47] A. L. Weisbrich, W. Simsbury, D. Rainey, and P. W. Olson, "WARP Solar/Wind Power: Green, User-Friendly and Cost Effective for the New Millennium International Power Markets," in *Proceedings of the American Power Conference*, 1999, pp. 232-237.

[48] V. Grigore, J. Hatonen, J. Kyyra, and T. Suntio, "Dynamics of a Converter with a Constant Power Load," 1998.

[49] A. Emadi and M. Ehsani, "Negative impedance stabilizing controls for PWM DC-DC converters using feedback linearization techniques," in *Energy Conversion Engineering Conference and Exhibit, 2000.(IECEC) 35th Intersociety*, 2000, pp. 613-620.

[50] J. W. Dixon, J. J. Garcia, and L. Moran, "Control system for three-phase active power filter which simultaneously compensates power factor and unbalanced loads," *Industrial Electronics, IEEE Transactions on,* vol. 42, pp. 636-641, 1995.

[51] X. Yan, "Control Strategies and Power Electronics in a Low-cost Electric Vehicle Propulsion System Employing a Brushless DC Machine," Northern Territory University, 2000.

[52] F. Krismer and J. W. Kolar, "Efficiency-optimized high-current dual active bridge converter for automotive applications," *Industrial Electronics, IEEE Transactions on,* vol. 59, pp. 2745-2760, 2012.

[53] B. M. Grainger, G. F. Reed, T. E. McDermott, Z.-H. Mao, V. Kounev, and D. Tipper, "Analysis of an offshore medium voltage DC microgrid environment—Part I: Power sharing controller design," in *T&D Conference and Exposition, 2014 IEEE PES,* 2014, pp. 1-5.

[54] A. F. Moreira, T. A. Lipo, G. Venkataramanan, and S. Bernet, "High-frequency modeling for cable and induction motor overvoltage studies in long cable drives," *Industry Applications, IEEE Transactions on,* vol. 38, pp. 1297-1306, 2002.

[55] L. Wedepohl and D. Wilcox, "Transient analysis of underground power-transmission systems. System-model and wave-propagation characteristics," *Electrical Engineers, Proceedings of the Institution of,* vol. 120, pp. 253-260, 1973.

[56] K. J. Åström and T. Hägglund, *Advanced PID control*: ISA-The Instrumentation, Systems, and Automation Society; Research Triangle Park, NC 27709, 2006.

[57] Y. Shamash, "Model reduction using the Routh stability criterion and the Padé approximation technique," *International Journal of Control,* vol. 21, pp. 475-484, 1975.

[58] K. Gu, J. Chen, and V. L. Kharitonov, *Stability of time-delay systems*: Springer Science & Business Media, 2003.

[59] M. Wu, Y. He, J.-H. She, and G.-P. Liu, "Delay-dependent criteria for robust stability of time-varying delay systems," *Automatica,* vol. 40, pp. 1435-1439, 2004.

[60] B. C. Moore and L. M. Silverman, "Model matching by state feedback and dynamic compensation," *Automatic Control, IEEE Transactions on,* vol. 17, pp. 491-497, 1972.

[61] M. Morari and E. Zafiriou, *Robust process control* vol. 488: Prentice hall Englewood Cliffs, NJ, 1989.

[62] G. S. Wood, R. O. Denoon, and K. Kwok, "Wind loads on industrial solar panel arrays and supporting roof structure," *Wind and Structures*, vol. 4, pp. 481-494, 2001.

[63] D. K. Decker and C. B. Loftis Jr, "Method of checking solar panel characteristics in an operating solar electrical system," ed: Google Patents, 1997.